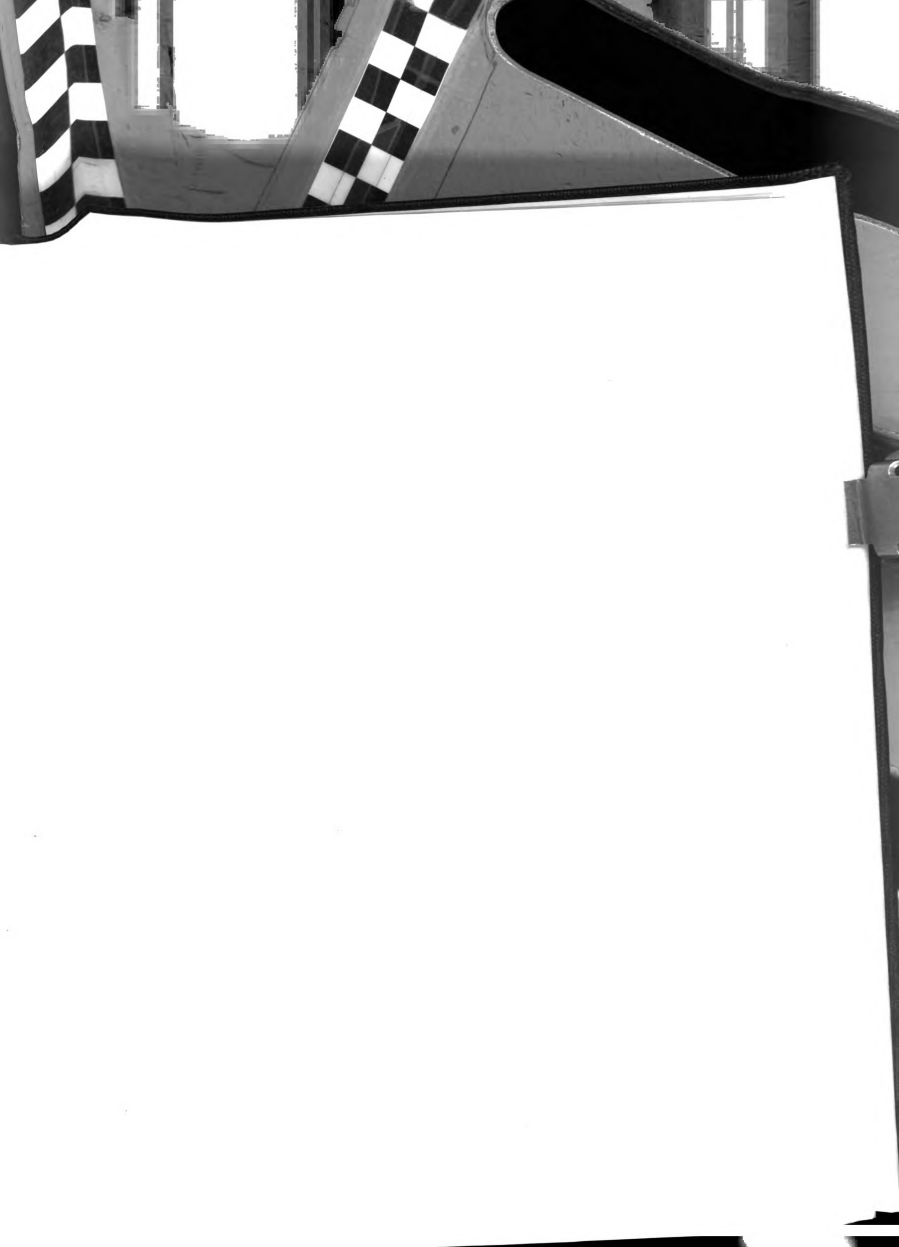

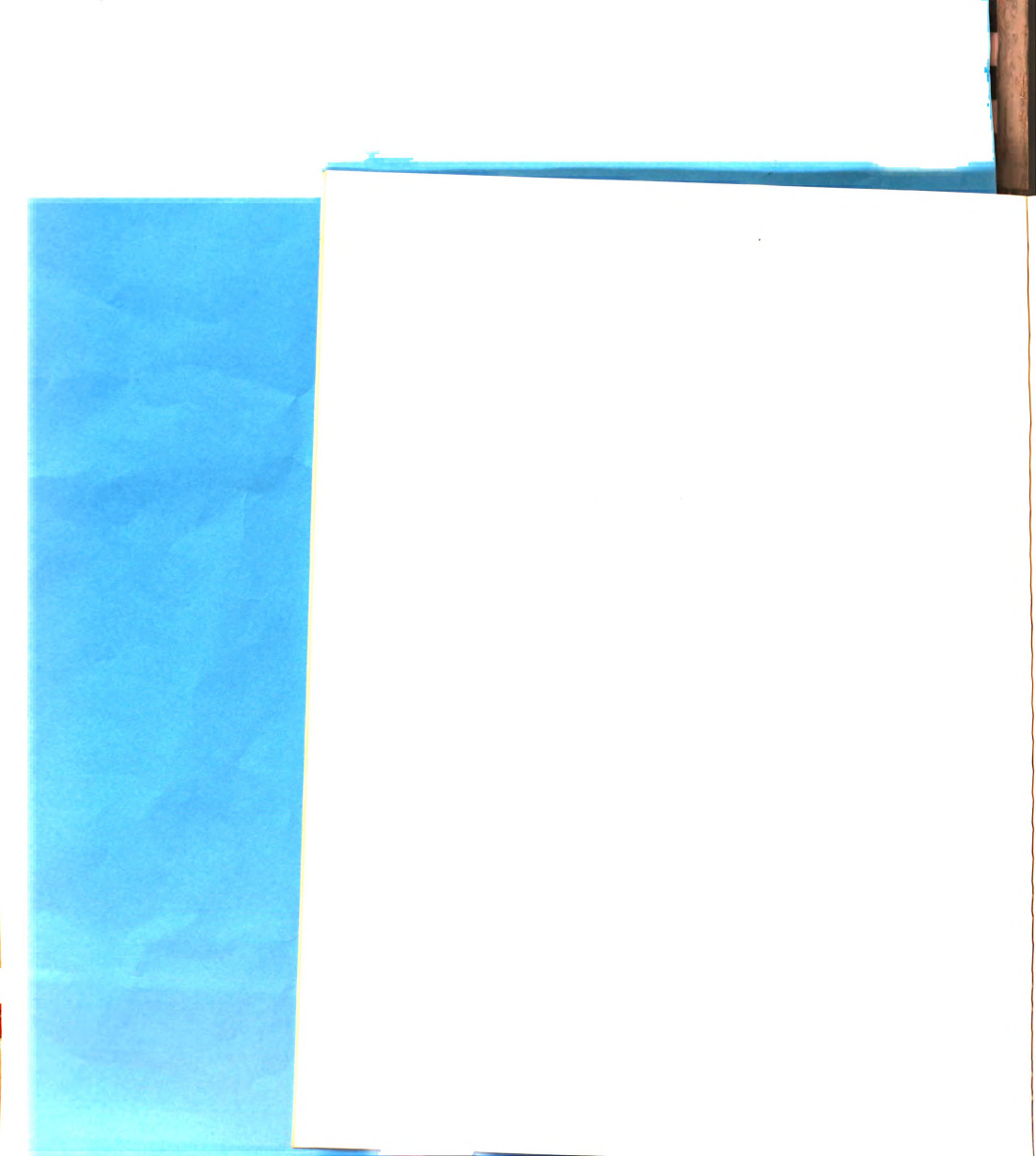

ABSTRACT

FAR INFRARED ABSORPTION IN THIN FILMS
OF PURE AND MIXED ALKALI HALIDES

by Richard M. Fuller

Experimental techniques were developed for the preparation and observation of thin evaporated films of pure alkali halides and of mixtures of alkali halides. Spectra were obtained in the neighborhood of strong infrared absorption. From the spectra the infrared dispersion frequency and the damping constant were obtained for the pure alkali halides. For LiI, the only alkali halide for which the infrared dispersion frequency had been measured neither by reflection or transmission, this parameter was found to be 144 cm^{-1}. For the other alkali halides, the values obtained were in very good agreement with those observed earlier by others in transmission measurements, and in good agreement with those deduced earlier from reflection measurements. The data are used to get a value of the effective charge e* according to Szigeti's formula. A correlation appears to exist between values of damping constant and deviation of e*/e from unity. Agreement between experimental values of e*/e and those predicted by theory can be said to be only fair.

With mixed films, composed of various proportions of LiBr with NaBr, LiCl with LiBr, and NaI with KI, the absorption spectra tended to have complex shapes, and only the infrared dispersion frequency could be determined. This parameter changes with composition and temperature.

The dispersion frequency shows a larger shift for a small proportion of the heavier component than that observed when the light constituent is the minority component. Also the absorption bands show much more broadening for the heavy minority component films than for light minority component films. For all of the systems studied, the absorption minimum becomes very broad and poorly defined as 50%-50% compositions are approached. The low temperature data from the NaI-KI system shows much sharper absorption at liquid-nitrogen temperatures as well as a shift of the dispersion frequency to higher values.

For the LiCl-LiBr system at intermediate compositions, a single band appears immediately after evaporation. Presently, the initial peak disappears and a new broader one appears with a minimum at a frequency about 60% of the initial minimum. This new minimum shifts monotonically with composition between the values of 201 cm^{-1} and 170 cm^{-1} for the pure LiCl and LiBr respectively.

FAR INFRARED ABSORPTION IN THIN FILMS OF PURE AND MIXED ALKALI HALIDES

By

Richard M. Fuller

A THESIS

Submitted to
Michigan State University
in partial fulfillment of the requirements
for the degree of

DOCTOR OF PHILOSOPHY

Department of Physics and Astronomy

1965

ACKNOWLEDGMENTS

Just as this thesis is the written evidence of a most valuable research experience, so are these words only written evidence of a feeling of profound appreciation for the contributions of many people who made this experience possible.

Dr. Donald J. Montgomery directed the work with the insight that made set backs as valuable as success. He has been an unfailing source of encouragement and counsel. The spirit of cooperation and excitement of the solid-state spectroscopy group is a tribute to the quality of leadership provided by Dr. Montgomery.

Dr. Charles M. Randall has provided invaluable assistance and counsel throughout the course of this work. He initially formulated the computer program used in the spectral analysis of this thesis. The example he set in experimental research will continue to serve as a model for the author.

Dr. Sitaram Jaswal was a valuable source of ideas and a sounding board for theoretical interpretations of the experimental work.

Karl Zetterholm did much of the important computer programing and organizing of data for analysis.

Gene Gardner punched data cards and cataloged spectra.

Alma College provided tangible support and a leave of absence in order to make this work possible.

The research has been supported by the Air Force Office of Scientific Research.

Finally, but most important, my wife, Judy, has been always a source of encouragement and has provided much assistance in the preparation of this thesis.

To these people and the many others who have assisted in this work, I express my appreciation.

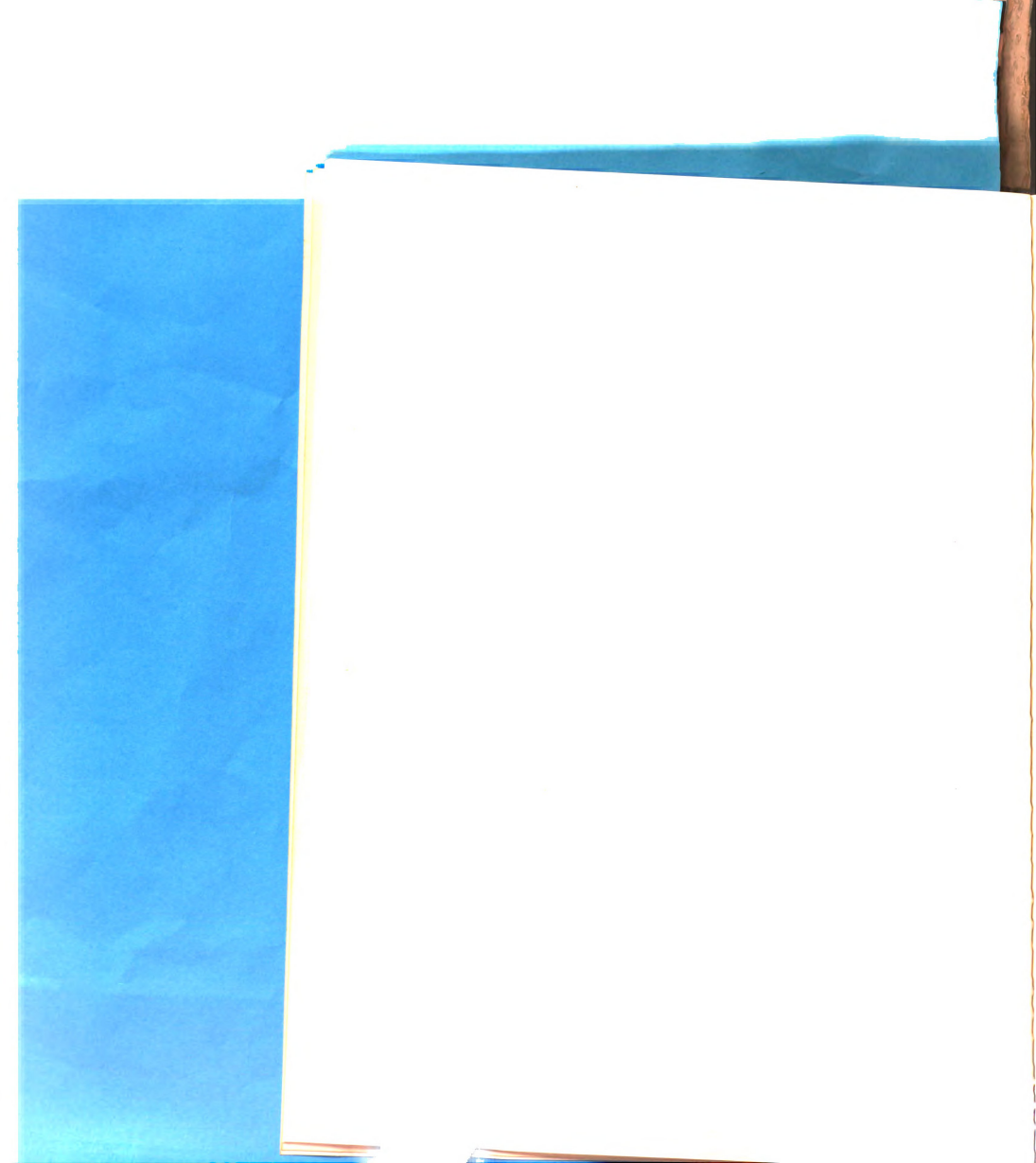

TABLE OF CONTENTS

LIST OF TABLES

LIST OF FIGURES

CHAPTER I

INTRODUCTION

Sir Isaac Newton's classic work of 300 years ago revealed the composite nature of white light. The many investigations since then have divided the electromagnetic spectrum into regions based on frequencies or wavelengths. Each of these regions has become the basis for a branch of the science of electromagnetic spectroscopy, wherein the scientist studies the energy levels of a material system through the interaction of electromagnetic radiation with it. Infrared radiation, usually defined as the region between wavelengths 1μ - 1000μ, or wavenumbers 10,000 cm^{-1} - 10 cm^{-1}, largely characterizes the interaction with the more massive and larger basic units of matter such as molecules and ions either individually, or as they are found collectively in gases, liquids, and solids.

Our understanding of the interaction of electromagnetic radiation with solids is far from complete. The collective system of particles making up a solid has held the theoreticians at bay, and we have no rigorous theory of absorption even for the simplest types of solids. Nor is there a systematic experimental study of this interaction. In our laboratory we have been concerned with experimental and theoretical investigations of the interaction between electromagnetic radiation and crystal-lattice vibrations in the region where the photon energies

are comparable with the phonon energies. In searching for a system where this interaction is strong, we were led to ionic crystals as were Czerny (1) and his followers some 30 years ago. The alkali halides, in particular, are excellent materials for a systematic investigation of the photon-phonon interaction, because of their large induced electric-dipole moments and simple structure.

In the absence of a rigorous theory we choose for our first-order model the simple picture of ions as charged mass points interconnected by approximately harmonic forces. This simple model needs to be improved to account for the shape of the absorption spectra, but refinements soon become complex and speculative. We have attempted to test these models in work carried out earlier in our laboratory by W.B. Zimmerman (2), R.H. Misho (3), and C.M. Randall (4), who have varied isotopic composition and temperature as experimental parameters in studies of infrared transmission through thin films of LiH and LiF.

The frequency of the maximum absorption by thin films of the ionic crystal is designated as the <u>infrared dispersion frequency</u>. The work of Zimmerman (2) and Misho (3) has shown that this characteristic frequency is essentially proportional to the reciprocal of the square root of the average reduced mass for the LiF films composed of different proportions of the isotopes Li-6

and Li-7 in combination with F-19. But in similar studies with H-1 and D-2 in combination with Li-6, an unexpectedly large shift in the dispersion frequency was observed for a small percentage of LiD in LiH. J.R. Hardy (5) has recently published a theoretical explanation for this phenomenon. He suggests, moreover, that alkali-halide mixed crystals might produce similar anomalous shifts in the dispersion frequency when a few per cent of the lighter host ions are replaced by heavier impurity ions.

The temperature dependence of the dispersion frequency is not taken into account in any simple model. Randall (4) has made a careful experimental study of this relationship for LiF from room temperature down to liquid-nitrogen temperatures. His results agree well with an effect estimated from Szigeti's relationship (6) between the dispersion frequency and the fundamental crystal-lattice parameters.

As might be expected, the absence of an adequate theory makes it difficult to get meaningful insights from the shapes of experimental absorption curves. Randall (4) has extracted an experimental half-width parameter from his data on LiF. So far as isotopic mass is concerned he found no significant differences in this parameter for Li^6F and Li^7F; he has observed a dependence on temperature, however, which needs further investigation. The effect of isotopic mixtures is to give much broader

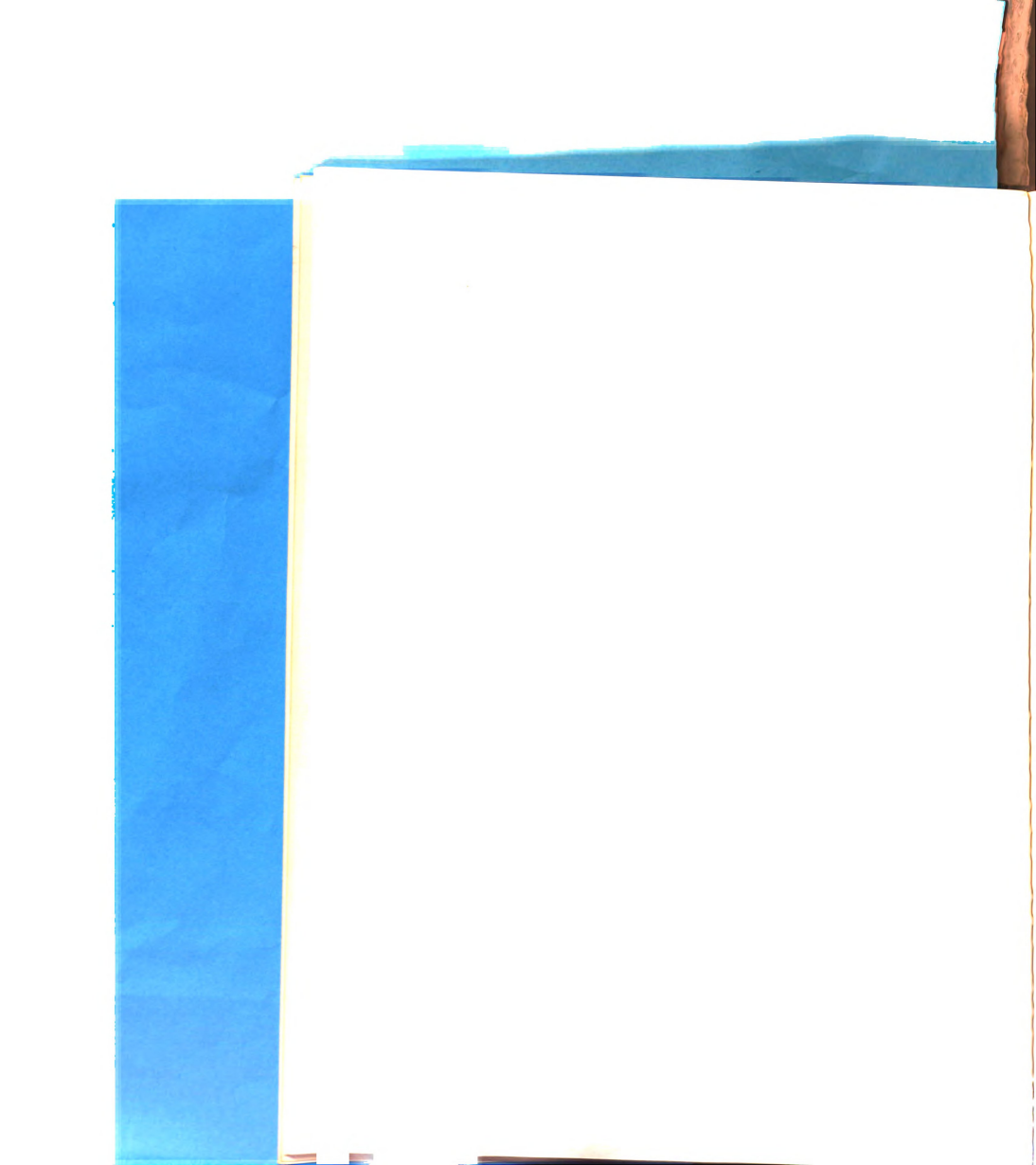

absorption bands than in pure films.

The present thesis consists of two series of experimental studies. The first part of the thesis is the determination of the dispersion frequencies for all of the alkali halides with NaCl structure. This study includes the determination of the dispersion frequency for LiI for the first time, and the first determinations for LiCl, LiBr, KF, RbF, and CsF by transmission measurements. This work provides a complete tabulation of NaCl-type alkali-halide dispersion frequencies. This study of pure films, moreover, serves to establish the soundness of the experimental technique, the purity of the materials, and the validity of the analysis. The second part of the thesis is a study of the infrared absorption of some films made from "pseudoisotopic" mixtures of alkali halides in which one alkali metal (or halogen) is replaced in part by another. The object of this study was to test this conception of "pseudoisotopicality" for the systems LiCl-LiBr, LiBr-NaBr, and NaI-KI, and to look for other effects due to finite concentrations of lattice impurities, as suggested by Hardy (5).

CHAPTER II

EXPERIMENTAL APPARATUS AND TECHNIQUE

The experimental method was practically the same for both the pure films and the mixed films. Any differences in techniques or apparatus will be specifically noted.

Sample Handling

All of the alkali halides studied in this work are hygroscopic to some degree or other. Consequently, certain precautions were taken to minimize absorption of water vapor from the atmosphere. First, the materials were stored in desiccators open to room atmosphere only during the brief periods necessary to load evaporator boats. To prepare mixed samples of desired composition, suitable amounts of pure materials were weighed and mixed in a dry box charged with dry argon. The amounts were weighed in a single-pan balance sensitive to 0.1 mg. The samples were mixed with an agate mortar and pestle, and then placed in weighing bottles which after sealing were removed from the dry box and placed in desiccators. All of the alkali halides used in this study were commercially obtained high-purity chemicals.

Evaporation Apparatus

A commercial evaporation system was used to prepare the films. The pumping system consists of a 15-cfm mechanical pump backing a 4" oil diffusion pump, with a

chevron-type liquid nitrogen baffle between the diffusion pump and the base plate. This system is capable of evacuating the bell jar to a pressure of 5μ Torr within 30 minutes.

The base plate is equipped with high-current feedthroughs and with two combination rotary-translational-motion feedthroughs. Currents up to 250 amp are supplied from a low-voltage transformer fed from a 15-amp variable autotransformer. One of the secondary leads of the low-voltage transformer served as a primary winding for an instrument transformer which monitors the current through the boat.

The experimental set-up for evaporation is shown in the schematic diagram of figure 1. The films were maintained in vacuo in two identical sample cells throughout the period of study. These cells, designed by W.B. Zimmerman, are described in detail by R.H. Misho (3). For the low-temperature studies, the substrate was mounted in a liquid-nitrogen container inside the vacuum cell. Figure 2 shows a cut-away view of the sample cell, with the liquid-nitrogen sample holder raised to clarify the construction. The top window was sealed to an O-ring by a brass holder as shown in figure 1. Throughout this study the material for the windows and the substrate was high-density polyethylene 0.40" thick. The second window, to be sealed after evaporation, was

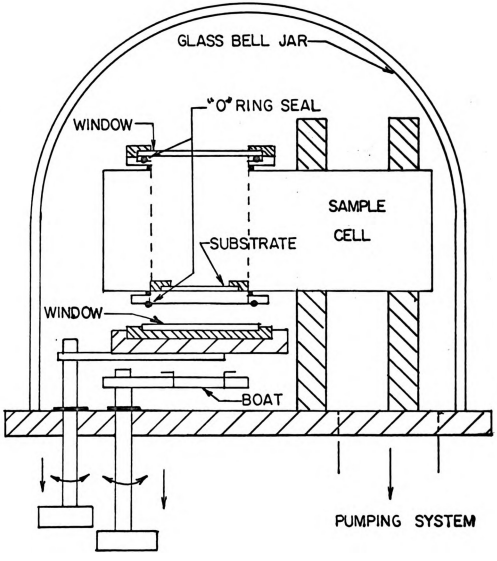

EVAPORATION SYSTEM

Figure 1

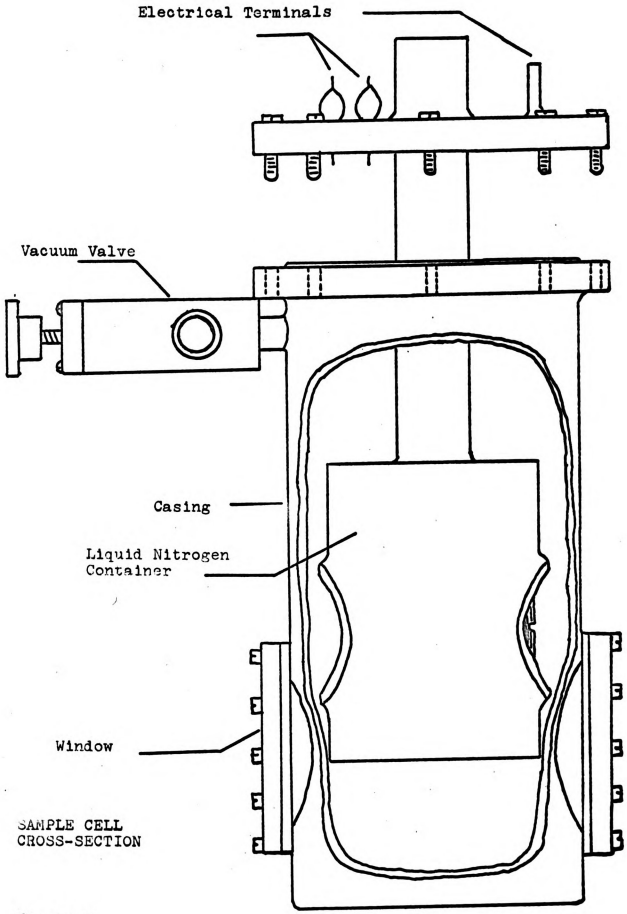
Electrical Terminals
Vacuum Valve
Casing
Liquid Nitrogen
Container
Window
SAMPLE CELL
CROSS-SECTION

Figure 2

placed in a holder mounted on one of the rotary feedthroughs in the vacuum system. The entire sample cell was aligned for the proper sealing of this window, and the cell was then secured by means of a mounting bracket rigidly mounted to the base plate.

Film Preparation

Small quantities of the material to be evaporated were placed in the boat. Each boat was made of molybdenum and mounted on an insulating support which in turn was mounted on the second rotary feedthrough of the vacuum system. The boat was connected to the high-current terminals in the base plate. The system was then evacuated, and the window mount on the rotary feedthrough was placed between the boat and the substrate mounted in the sample cell (see figure 1). This window mount served as a shield for the substrate during the period of preheating before evaporation. The preheating of the material in the boat was monitored by means of the pressure of the system as measured on an ion gauge. The pressure usually stabilized after heating for a few minutes. This period of outgassing is very important when dealing with the hygroscopic materials used in this study. Without this precaution some of the evaporant sputters out of the boat, and useful films are not obtained. After the period of preheating, the current to the boat is raised until the powder melts. As part of this study, the substrate

shield was removed at different times during evaporation. The resulting films from the different portions of the evaporation produced no observable differences in their transmission spectra. The period of evaporation was approximately 20 seconds with the boat 10 cm from the substrate, and with a boat current of 100 amp. After the current to the boat was turned off, the window holder was rotated into position and the window was pressed firmly against the O-ring in the sample cell (see figure 1). Air was admitted to the bell jar. The pressure difference between atmosphere and the inside of the sample cell sealed the polyethylene window in its position, thus maintaining the film in a vacuum inside the sample cell. The cell was then removed from the mounting bracket in the evaporator and placed in the sample compartment of the Perkin-Elmer 301 spectrophotometer. Hose connections were made between the sample cell and forepump, so that the cell could be pumped on at any time during the experiment. With this arrangement the pressure inside the sample cell could be maintained below 10^{-3} Torr throughout the course of an experiment.

The output from a copper-constantan thermocouple was fed into a Daystrom-Weston multiple-station self-balancing recording potentiometer to measure the temperature of the substrate for the low-temperature runs. The thermocouple junction was clamped firmly against the high-density

polyethylene substrate. Randall (4) ascribes to similar thermocouple temperature measurements an accuracy of ± 1 deg-C at liquid-nitrogen temperature, and a higher accuracy at room temperature.

Transmission-Spectra Measurements

The transmission spectra of the films were obtained with a commercial double-beam far-infrared spectrophotometer, the Perkin-Elmer Model 301. A diagram of the optical path of the instrument is shown in figure 3. Between the source at I and the Golay detector, several of the reflection elements, the transmission filters at F3, and the crystal choppers may be changed in order to isolate a narrow band of the electromagnetic spectrum for dispersion by the grating G1. The mechanical drive for the grating is designed so that the frequency of the radiation passed by the monochromator is directly proportional to the number of drive-shaft turns, which is based on an arbitrary scale of 100 "drum turns" per revolution. The "drum turns" scale was calibrated in terms of frequency for each grating by operating the instrument in the single-beam mode, and measuring the positions of the absorption bands of atmospheric water vapor. The frequencies of these bands are tabulated in the literature (7), and a straight line between these values and the experimental data was fitted by the

Figure 3. Optical path of the Perkin-Elmer 301 far-infrared spectrophotometer. Reflection elements on F1, F1', and F2 may be changed from outside the instrument. Mirrors M4, M4', and M12 along with the choppers may also be changed to isolate a band of the electromagnetic spectrum for dispersion by the grating G1 before being detected by the Golay cell near M22.

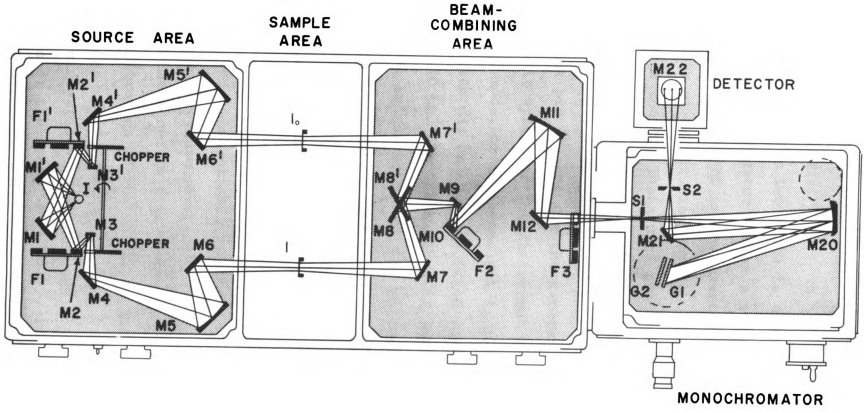

DOUBLE - BEAM FAR - INFRARED SPECTROPHOTOMETER

Figure 3

method of least squares.*

The ratio of the two beams is displayed on a digital-readout indicator and on a strip-chart recorder. The position of the pen on the chart is correlated with the position of the grating through pips on the edge of the recorder chart. These pips are made by a microswitch-pen system synchronized with the grating-wavenumber drive. A pip appears for every drum-turn number ending in zero, and an extra pip appears for the numbers ending in 95.

The slit system of the instrument may be operated in a manual mode, or in a constant-I_0 mode. In the manual mode the slits may be set to a fixed width up to a maximum opening of 10 mm. In the constant-I_0 mode, a constant signal level is maintained in the reference beam by adjusting the slit width by means of a servomechanism. To minimize the signal fluctuations due to atmospheric

---

* A recent paper (8) gives a list of more precise values for the atmospheric absorption lines as found with a Perkin-Elmer 301 spectrophotometer. The differences between the frequencies assigned in this paper and those taken by us for the calibration of the gratings used in this study are less than 0.25 cm^{-1}. These differences are unimportant in the study of lattice-vibration spectra which show broad half-widths of the order of 25 cm^{-1}.

absorption, the instrument is continuously purged with dry nitrogen.

The two sources available for the instrument were used in this study. A Globar operating at about 200 watts power input was the source for spectra in the wavenumber range 300 cm^{-1} to 125 cm^{-1}, and a high-pressure mercury arc was the source in the range 125 cm^{-1} to 50 cm^{-1}. The dispersive element was a 20-line/mm grating with the Globar as the source, and an 8-line/mm grating with the mercury source.

The amplifier gain was adjusted to give a slit width of about 5.0 mm in the region of the absorption maximum. This geometric slit width corresponds to a spectral slit width of about 1 micron. The correction for this spectral slit width is negligible.

The records of the stray light for the wavenumber ranges 250 cm^{-1} to 145 cm^{-1}, and 145 cm^{-1} to 55 cm^{-1} should be less than 2% and 4% respectively.

The damping in the various servomechanisms is adjusted so that little noise is apparent in the recorder trace. The damping required for this type of spectrum must be coupled with a slow scanning speed in order to keep the tracking error small. The spectra were scanned at the rate of 7.73 cm^{-1}/min. or slower. Figure 4 is a typical reference spectrum for the sample cell. No change was noted

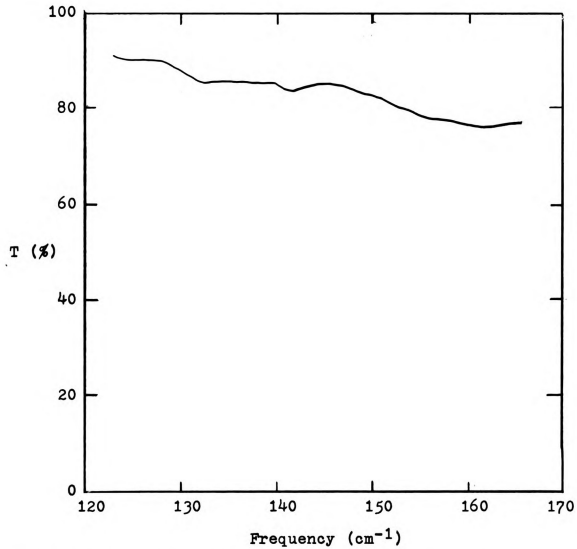

Figure 4 A reference spectrum for the sample cell

in the reference spectrum of the sample cell at liquid-nitrogen temperatures.

Spectral Analysis

Analysis for Pure Alkali-Halide Films: In the usual manner the dispersion frequency, ω_o, is defined experimentally as the limit of the position of the absorption peak as the film thickness approaches zero. If we use films sufficiently thick to overcome instrumental limitations, we must adopt some model that enables us to extract ω_o from the observed spectrum. We have chosen the phenomenological model, proposed initially by Lorentz, consisting of a single dispersion oscillator of frequency ω_o and damping constant γ. On this model the dielectric constant ϵ at a frequency ω is:

$$(1) \quad \epsilon(\omega) = \epsilon_\infty + (\epsilon_o - \epsilon_\infty) \Big/ \left\{1 - (\omega/\omega_o)^2 - i\left(\gamma/\omega_o\right)\left(\omega/\omega_o\right)\right\}$$

where ϵ_o is the static dielectric constant, and ϵ_∞ is the high-frequency dielectric constant (visible region). For a plane parallel film of thickness d with a complex refractive index $\bar{n} = \epsilon^{1/2}$, the transmission T for electromagnetic radiation of frequency ω is:

$$(2) \quad T = \left| 4\bar{n}\, e^{-i\frac{\omega d}{c}} \Big/ \left\{(1+\bar{n})^2 e^{-i\frac{\bar{n}\omega d}{c}} - (1-\bar{n})^2 e^{i\frac{\bar{n}\omega d}{c}}\right\} \right|^2$$

It is readily shown that as d goes to zero, T approaches a minimum at $\omega = \omega_o$. The problem of spectral analysis becomes that of selecting the "best" values for the

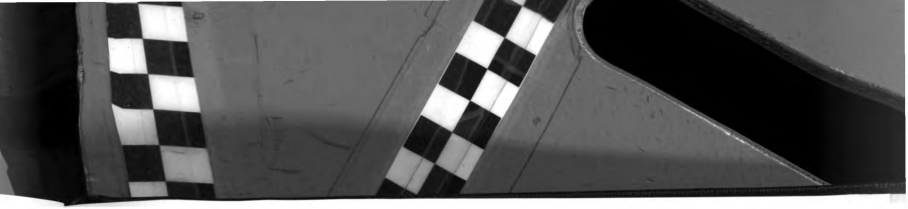

parameters to fit the observed curve with the equation resulting from the substitution of (1) into (2). Taking ϵ_o and ϵ_∞ from the literature, we choose values for d, γ , and ω_o so as to minimize the integral of the square of the deviation between the adjusted experimental spectrum and the computed curve. For this purpose selected points from photographs of spectra from the spectrophotometer are entered on punched cards with the aid of a Hydel scanning machine employing a Datex encoder system. These cards are used as input for a CDC-3600 computer. The computer is programmed first to determine the adjusted experimental spectrum by dividing the input spectrum by the appropriate reference spectrum, and next to yield the best-fit values of the parameters d, γ , and ω_o . The computer also plots the adjusted experimental spectrum and the calculated curve. Figure 5 shows the result for a LiBr spectrum. The solid curve is the adjusted experimental spectrum, and the dashed curve is the calculated spectrum.

Analysis for Mixed Alkali-Halide Films: There are no experimental values for ϵ_o and ϵ_∞ for the mixed alkali-halide films used in this study. Therefore, for the mixed-film spectra the analysis problem degenerates to simply determining the frequency of the transmission minimum. This determination was made by a computer search of the

Figure

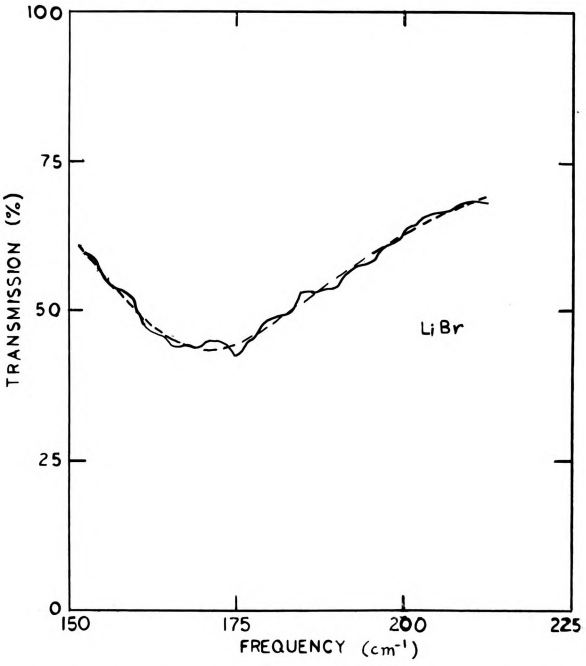

Figure 5 Absorption spectrum for LiBr. The solid line is the corrected experimental spectrum, and the broken line is the computer calculated spectrum.

adjusted experimental spectrum, and by graphical analysis. The computer search consisted of finding the minimum sum of five consecutive data points, and then assigning the middle point as the spectrum minimum. In all cases the agreement between computer search and the graphical analysis was excellent.

Exper

deter
the a
These
transm
concer
disper
Randal
of dis
obtain
analys
first
LiCl,
These
togeth
agreem
of pre
freque
valida
with t
even t
with t
each c
appen

CHAPTER III

Experimental Results and Discussion

The first part of this study consisted of the determination of the dispersion frequencies for all of the alkali-halides having the NaCl crystal structure. These frequencies were determined from thin-film transmission data, as explained in the previous section concerning spectral analysis. The values of the dispersion frequencies from this study and from that by Randall (4) for LiF provide the most complete tabulation of dispersion frequencies for the alkali halides as obtained with common experimental techniques and spectral analysis. Moreover, this investigation constitutes the first determination of the dispersion frequencies for LiCl, LiBr, LiI, KF, RbF, and CsF by transmission. These dispersion frequencies are given in table I, together with previous data where available. The agreement between the results of this study and those of previous transmission measurements of the dispersion frequencies is very good. This agreement serves to validate the technique. Some disagreement exists, however, with the reflection data of Hass (9) for LiCl and LiBr, even though his data for KF and RbF agree quite well with the data reported here. An actual spectrum for each of the alkali-halide films studied is given in the appendix.

Table I

Experimental Data for Pure Films

	This Study		Previous Work		
Material	ω_o (cm^{-1})	γ/ω_o	ω_o (cm^{-1})	γ/ω_o	Reference
LiF			306	0.09	(4)
LiCl	201± 2	0.20	191		(9) *
LiBr	170± 2	0.25	159		(9) *
LiI	144± 2	0.38			
NaF	246± 2	0.10	239		(11)
NaCl	164± 1	0.10	164		(1)
NaBr	135± 1	0.09	135	0.07	(10)
NaI	115± 1	0.16	116	0.18	(10)
KF	191± 2	0.12	190		(9) *
KCl	142± 2	0.10	144	0.05	(10)
KBr	115± 1	0.08	116	0.06	(10)
KI	101± 1	0.07	102	0.07	(10)
RbF	156± 2	0.23	156		(9) *
RbCl	118± 1	0.07	119	0.08	(10)
RbBr	88± 1	0.08	89	0.06	(10)
RbI	76± 1	0.12	75	0.06	(10)
CsF	127± 2	0.20			
CsCl	101± 1	0.11	99	0.10	(10)
CsBr	74± 1	0.05	74	0.08	(10)

* Data obtained from reflection measurements

Table I contains also the values of the half-width parameter γ/ω_0, extracted from the data as described earlier. These values may be compared with the values reported by Jones, et al. (10); again the agreement is quite good, particularly in view of the fact that the methods of extracting this parameter from the experimental data are different.

The damping term is introduced ad hoc in the theory as developed by Born and Huang (14). The atomic origins of this damping are thought to be 1) anharmonic terms in the lattice potential, and 2) higher-order induced-dipole-moment terms. Qualitatively then, we will associate larger values of γ/ω_0 with greater importance of these two factors in the theorectical picture of our system. We will have occasion later to make use of this correlation.

From the classical theory of dielectric constants for ionic crystals, Szigeti (6) has developed the following equation relating the dispersion frequency to other experimental parameters:

(3) $\epsilon_o - \epsilon_\infty = (\epsilon_\infty + 2)^2 \left[4\pi N (Ze)^2\right] / 9 \bar{M} \omega_o^2$

where ϵ_∞ is the high-frequency dielectric constant, ϵ_o is the low-frequency dielectric constant, ω_o is the infrared dispersion frequency, N is the number of ion pairs per unit volume, Ze is the ionic charge, and $\bar{M}$ is the reduced mass of the positive and negative ion pair. Equation (3) is not satisfied by the experimental data. Consequently Szigeti (6) introduced an effective charge e* in place of e in this relation. Then the ratio of e*/e is given by

(4) $(e^*/e)^2 = 9 \bar{M} \omega_o^2 (\epsilon_o - \epsilon_\infty)/4\pi N e^2 (\epsilon_\infty + 2)^2$ (for Z =1)

Thus the difference between the ratio e*/e and unity serves to show the discrepancy of the classical model with respect to the experimental data. Table II compares the ratios of e*/e as calculated by equation (4) with this ratio as predicted from other models. The discrepancies between experimental data and the simple theoretical models have been confirmed by previous studies. Jones et al.(10), in particular, have shown that these differences do not disappear even at liquid-helium temperatures where the models are more likely to be valid.

TABLE II

Comparison of e*/e Values

Material	Szigeti	Havinga	Dick & Overhauser e*/e	Dick & Overhauser (e*/e)extreme
LiF	0.81	0.77	0.91	0.88
LiCl	0.77	0.67	0.92	0.90
LiBr	0.77	0.71	0.91	0.90
LiI	0.55	0.52	0.90	0.88
NaF	0.95	0.85	0.93	0.86
NaCl	0.74	0.68	0.91	0.84
NaBr	0.70	0.71	0.89	0.82
NaI	0.70	0.64	0.89	0.83
KF	0.88	0.83	0.98	0.87
KCl	0.80	0.80	0.93	0.84
KBr	0.77	0.81	0.93	0.84
KI	0.71	0.74	0.91	0.82
RbF	0.95	0.71	1.05	0.88
RbCl	0.83	0.76	0.95	0.84
RbBr	0.83	0.80	0.92	0.83
RbI	0.76	0.76	0.93	0.85
CsF	0.86	0.89		
Mean deviation From Szigeti Value		0.056	0.134	0.082

There have been a number of theoretical discussions concerning the origin of these deviations of e*/e from unity, and we now discuss our results in light of these. The three main factors affecting the value of e*/e that are not accounted for in the simple theory are 1) ionic overlap, 2) ionic distortion, and 3) anharmonic forces. The shell model, first proposed by Dick and Overhauser (12), is an attempt to correct for overlap and ionic distortion in determining the ratio of e*/e. Havinga (13) has modified this model, and in Table II the theoretical values of e*/e based on each of these papers are compared with those determined from the experimental data and the Szigeti formula.

The shell model may be qualitatively understood in the following way. An ion is assumed to consist of a spherical shell of n outermost electrons and a core consisting of the nucleus and tightly-bound inner electrons. In an applied electric field the shell is assumed to maintain its spherical shape, and to move with respect to the core. A harmonic restoring force acts between the core and the shell. Now, the shells of the positive and negative ions repel each other and tend to become displaced with respect to the ion cores because of this repulsion. This displacement represents a short-range polarization of the ions. Since the restoring force in the larger negative ions is in general weaker than that

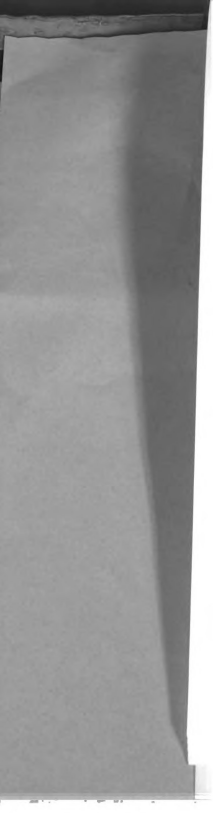

in the positive ions, we expect the short-range polarization of the negative ion to exceed that of the positive ion (if shell charges are the same). Thus there is a net dipole per ion pair directed opposite to the applied field, and this contribution serves to lower e*/e (i.e. to reduce the total dipole moment) below unity.

The results in Table II show that the shell model accounts for some of the disagreement between the experimental data and the simple theory. Havinga's values are in general closer to the experimental values, but one would hope for still better agreement.

We note a correlation between larger values of γ/ω_0 in Table I, and the larger deviations of e*/e from unity in Table II. This correlation, which is consistent with taking ionic overlap effect as one of the origins of the damping, might prove to be a valuable area for further studies, in which one would seek an inclusive theoretical description of the interaction of electromagnetic radiation with ionic crystals.

Mixed-Film Results

Three systems of mixed alkali-halide films were studied: LiBr-NaBr, LiCl-LiBr, and NaI-KI. Films were made of several different molecular percentages for each of the three systems. The frequency of minimum transmission was determined for each film as previously described. This frequency will hereinafter be called the mixed film

dispersion frequency. These dispersion frequencies are reported along with the values for the pure-film dispersion frequencies for each of the systems studied. Specific comments will be made for each system in turn, and a general discussion for all of the mixed-film results will follow.

LiBr-NaBr System

Figures 6 to 14 show spectra for various compositions of the LiBr-NaBr system. A plot of the dispersion frequencies for various compositions is shown in figure 15. There are three observations to be made for this system; first, the absorption maximum becomes broader and more poorly defined as the composition of the melt approaches 50%-50%; second, the dispersion frequency changes more for a small percentage of NaBr in LiBr than it does for the same percentage LiBr in NaBr; third, a small percentage of NaBr in LiBr changes the shape of the spectra much more than the same percentage of LiBr in NaBr (cf. figures 8 and 13).

LiCl-LiBr System

Figures 16 to 22 show spectra for different compositions of the LiCl-LiBr system. In figure 23 both the initial and the final values of the dispersion frequency are plotted for each of the different mixed films. The initial value of the dispersion frequency is that taken from the first spectrum obtained following

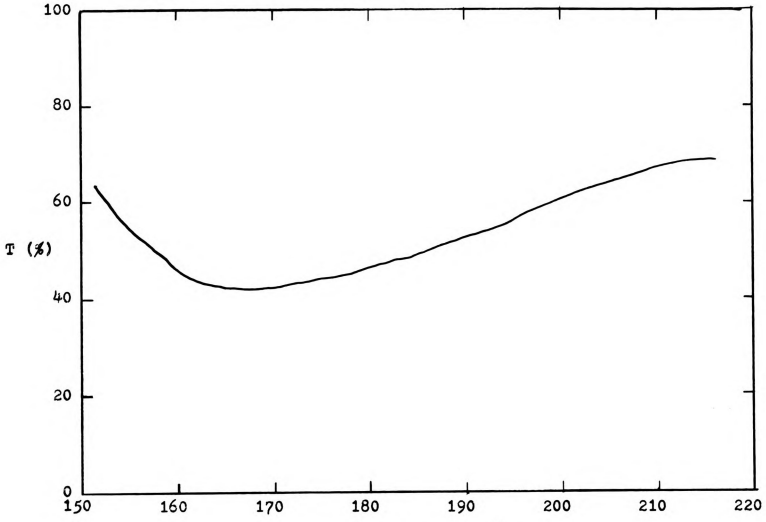
100
80
60
40
20
0
T (%)
150
160
170
180
190
200
210
220
Frequency (cm^{-1})
LiBr

Figure 6

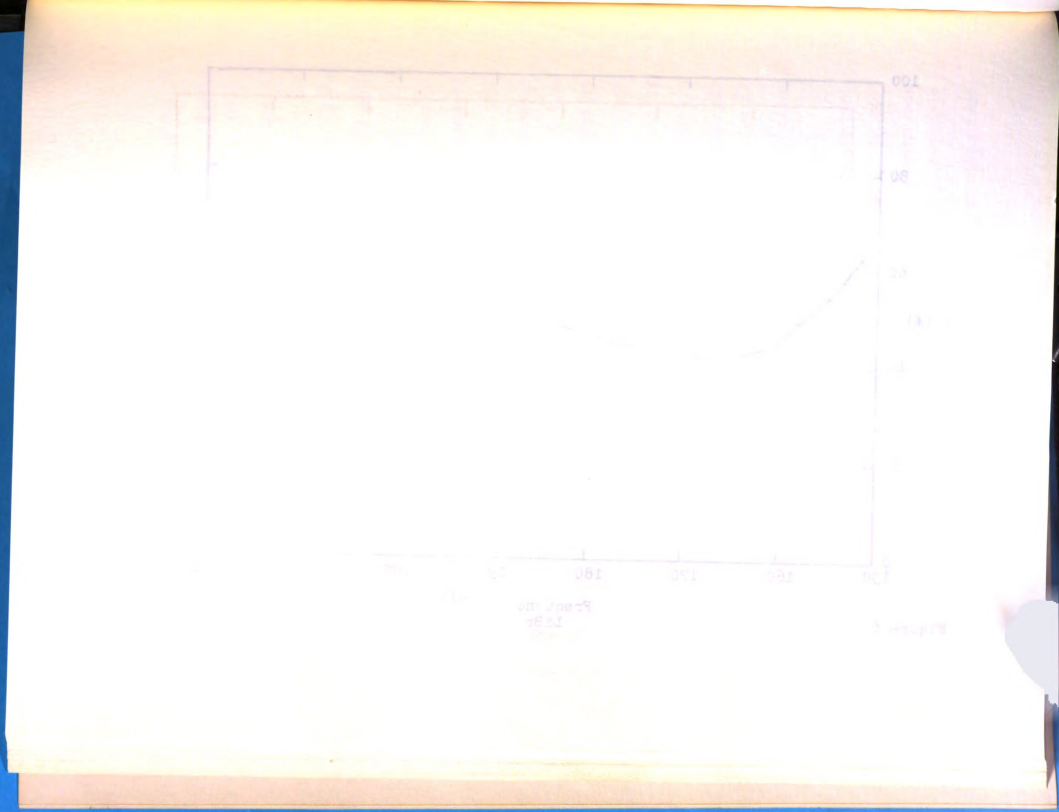

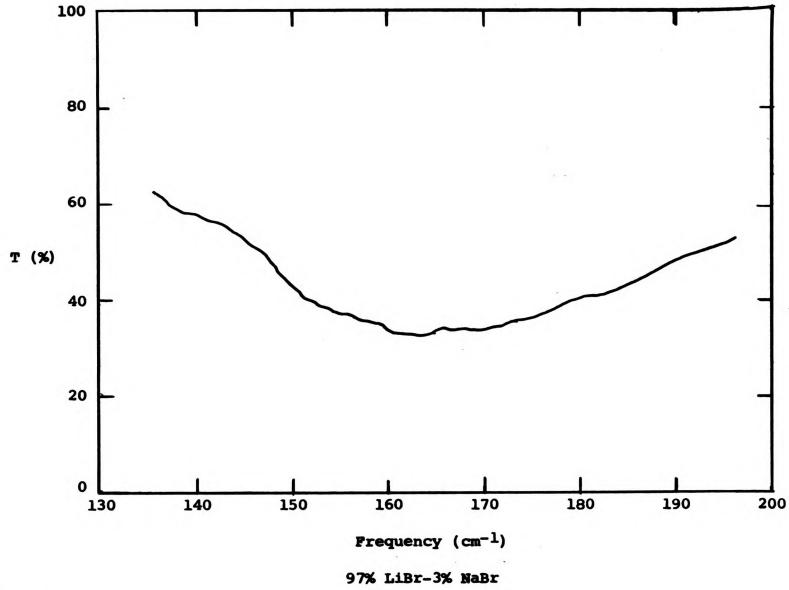
100
80
60
40
20
0
T (%)
130
140
150
160
170
180
190
200
Frequency (cm-1)
97% LiBr-3% NaBr

Figure 7

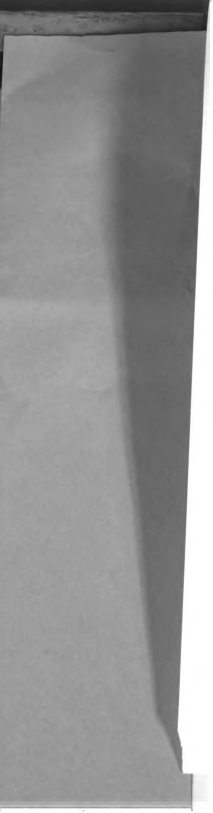

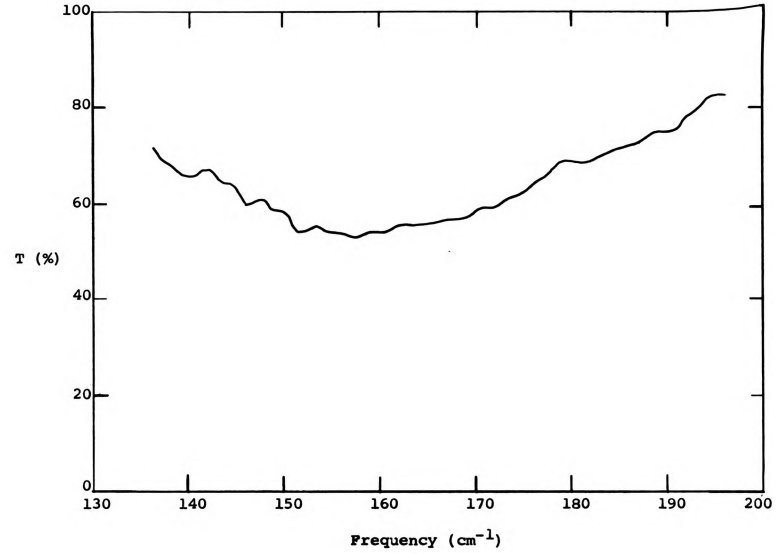
100
80
60
40
20
0
T (%)
130
140
150
160
170
180
190
200
Frequency (cm^{-1})
90% LiBr-10% NaBr

Figure 8

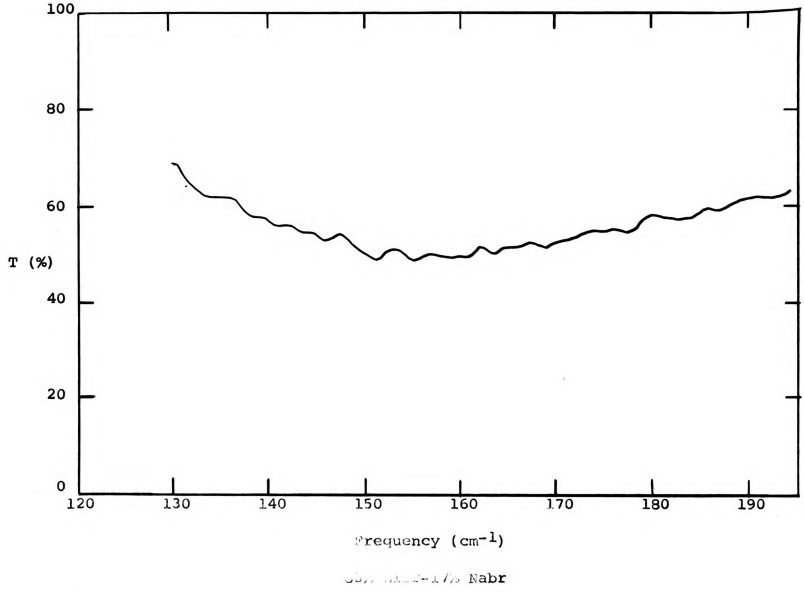

Figure 9

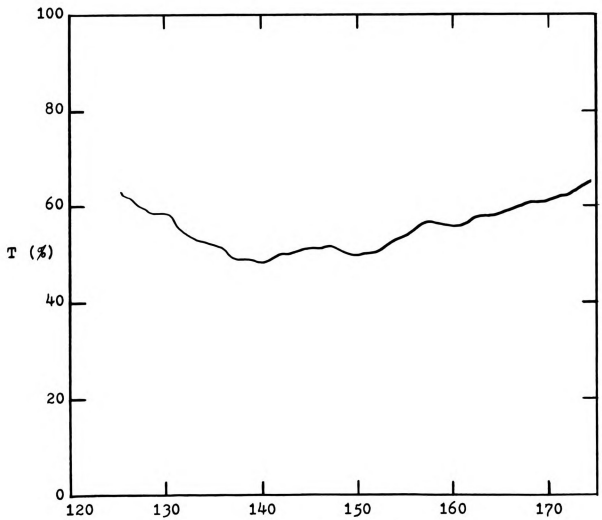

50% LiBr-50% NaBr

Figure 10

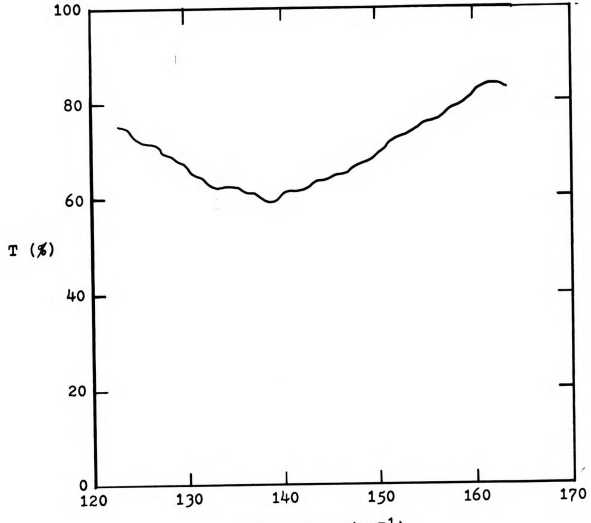
100
80
60
40
20
0
T (%)
120
130
140
150
160
170
Frequency (cm^{-1})
30% LiBr-70% NaBr

Figure 11

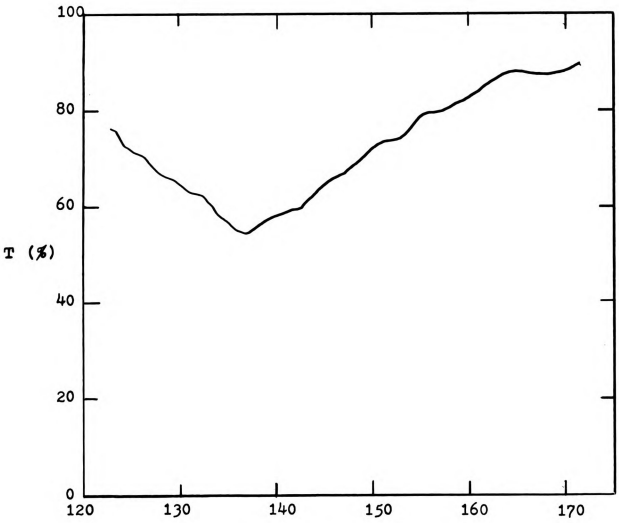

21% LiBr-79% NaBr

Figure 12

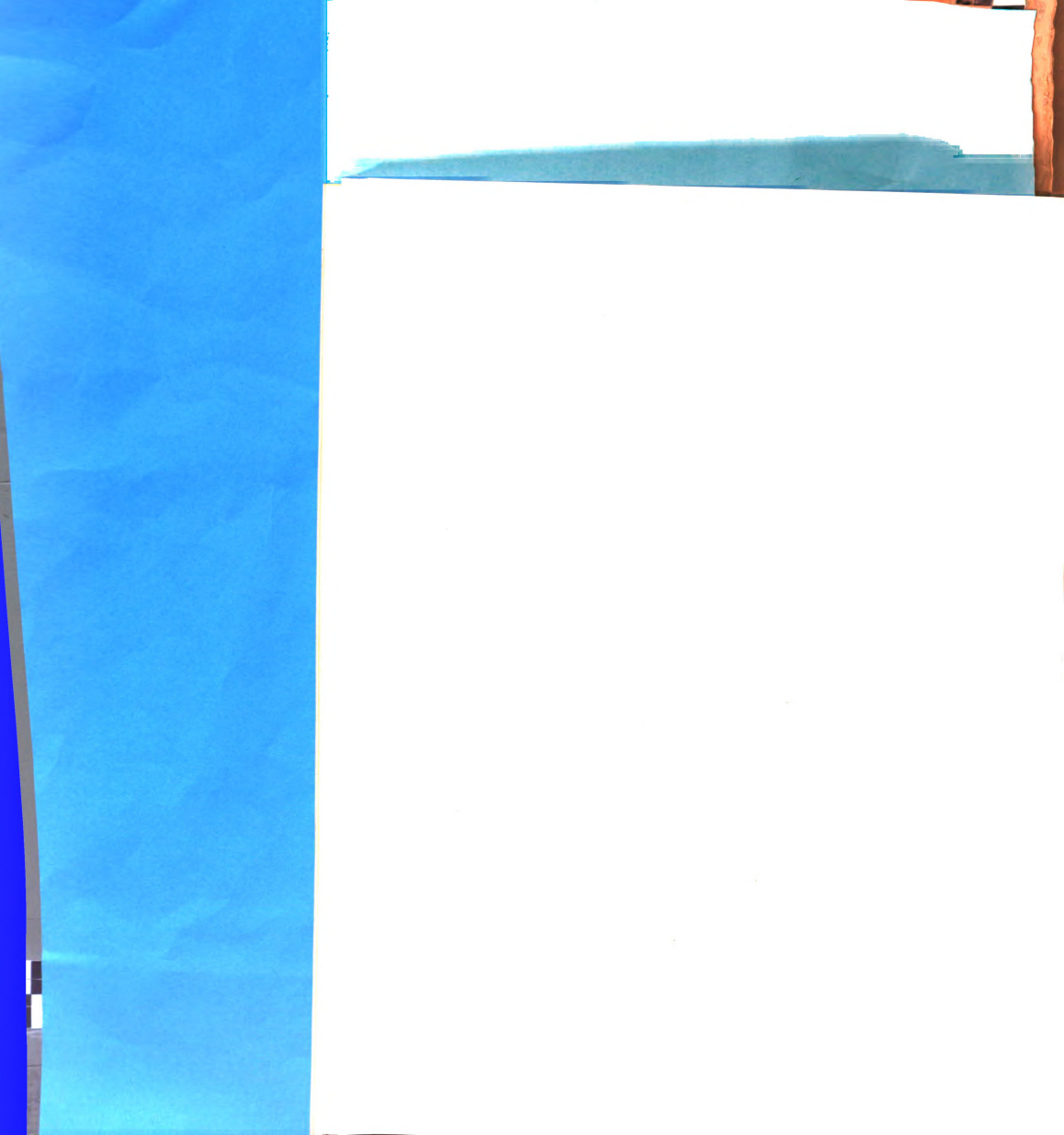

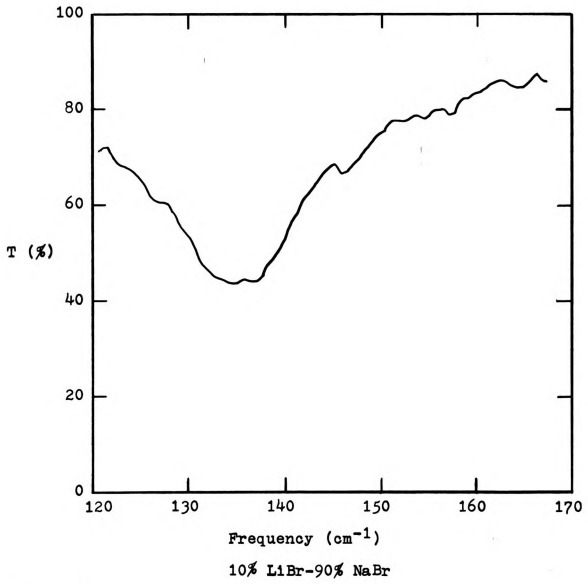

10% LiBr-90% NaBr

Figure 13

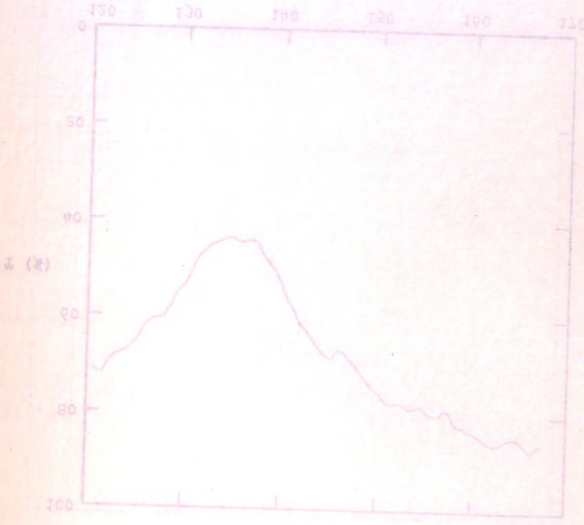
0
50
100
150
200
250
300
350
T (K)

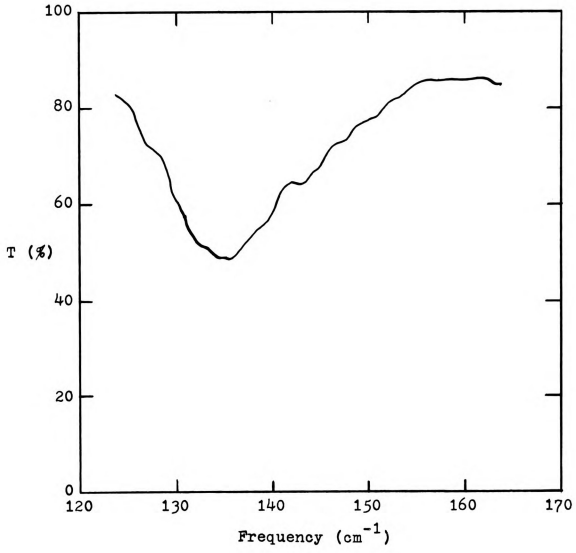

NaBr

Figure 14

100
80
60
40
20
0
T (K)
150
140
130
120
110

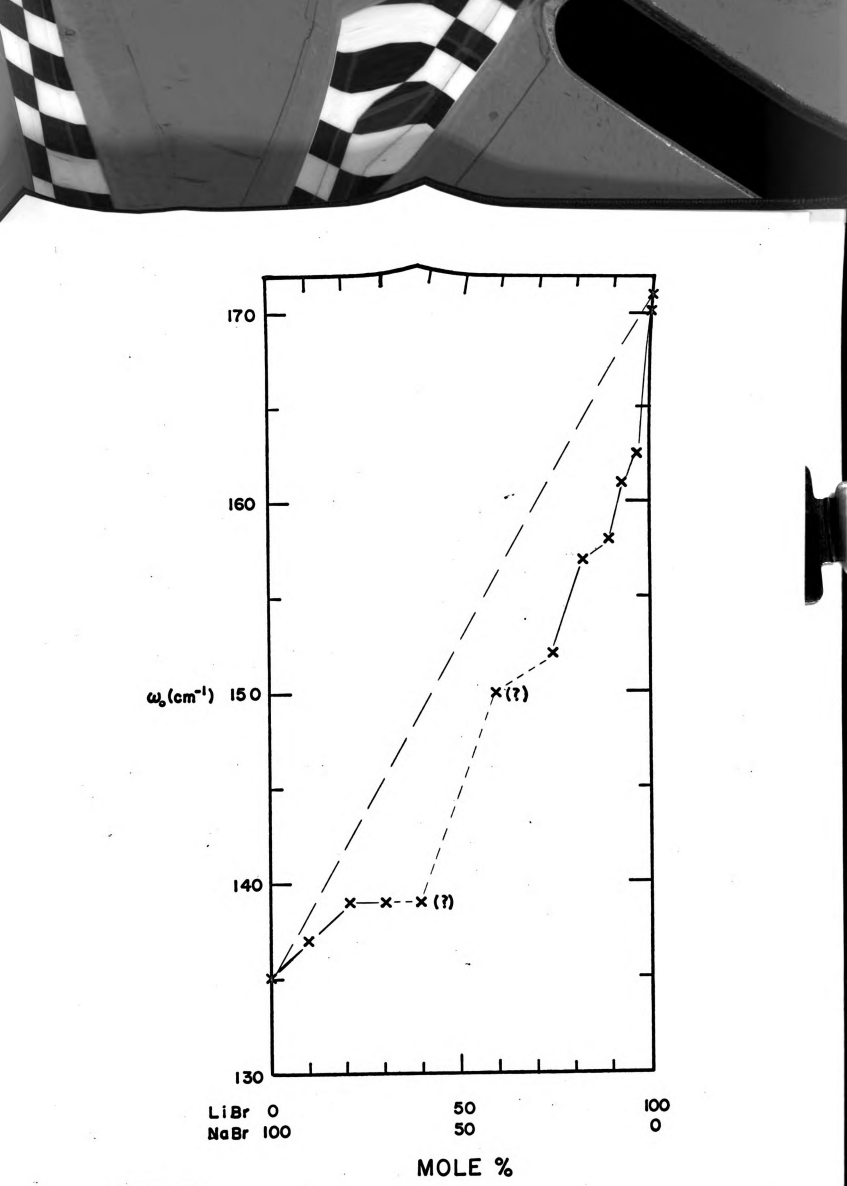

Figure 15

evaporation of the film. Instead of lying between the dispersion frequencies of the pure films as expected, this initial frequency is much higher than that of pure LiCl films. After a period of from several minutes to several hours during which the film is maintained in vacuo, a new spectrum appears, revealing the dispersion frequency shifted to a lower value that lies between the dispersion frequencies for pure films. Such a final equilibrium value for the dispersion frequency was found for all of the films having the melt compositions 80% LiCl- 20% LiBr, 60%-40% LiCl-LiBr, and 40%-60% LiCl-LiBr. The 21% LiCl-79% LiBr composition never produced a spectrum with such an initially high value of the dispersion frequency. The spectra (see figures 16 and 17) show that the initial absorption peak is usually better defined than the final one. Moreover, the absorption peak is broader for films from 60%-40% combinations than for 80%-20% combinations.

NaI-KI System

Several spectra for different compositions of the NaI-KI system are shown in figures 24 to 30. Each figure shows spectra at room temperature ($\sim 300^{\circ}$K) and liquid-nitrogen temperature ($\sim 110^{\circ}$K film temperature) for the same film. A plot of the dispersion frequencies for various compositions at room temperature and liquid-nitrogen temperature is shown in figure 31. Since this

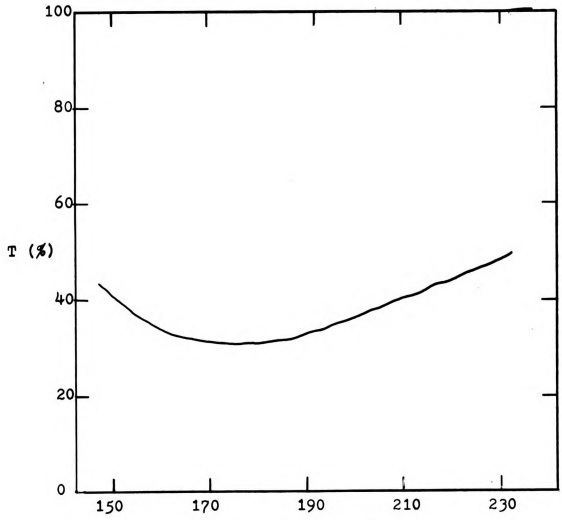

79% LiBr-21% LiCl

Figure 16

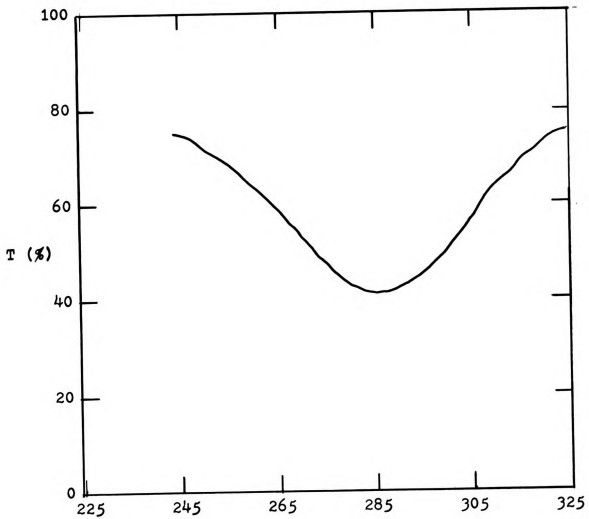

(Initial)

60% LiBr-40% LiCl

Figure 17

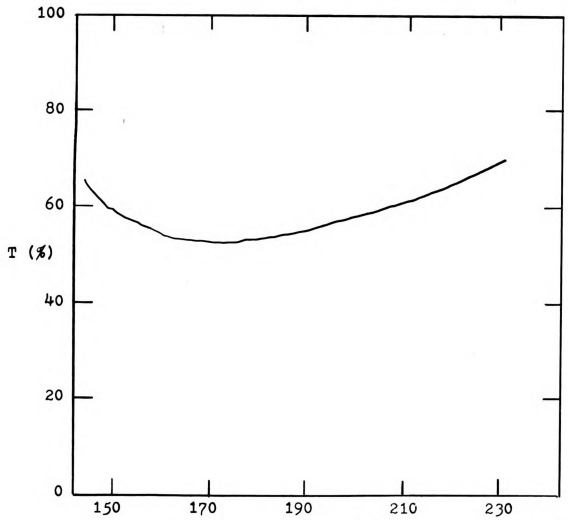

(Final)

60% LiBr-40% LiCl

Figure 18

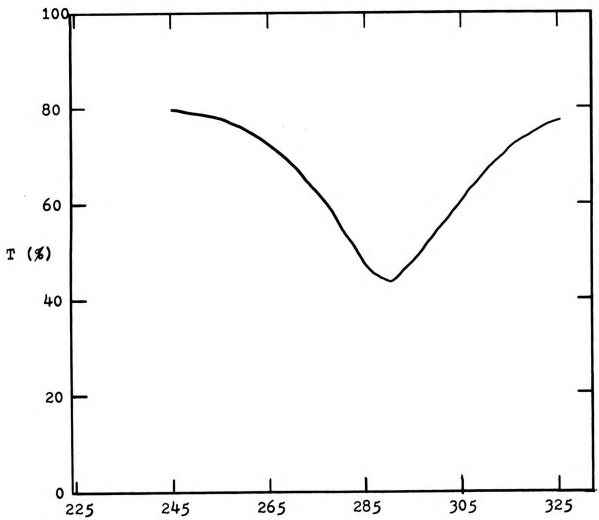
100
80
60
T (%)
40
20
0
225
245
265
285
305
325
Frequency (cm^{-1})
(Initial)
40% LiBr-60% LiCl

Figure 19

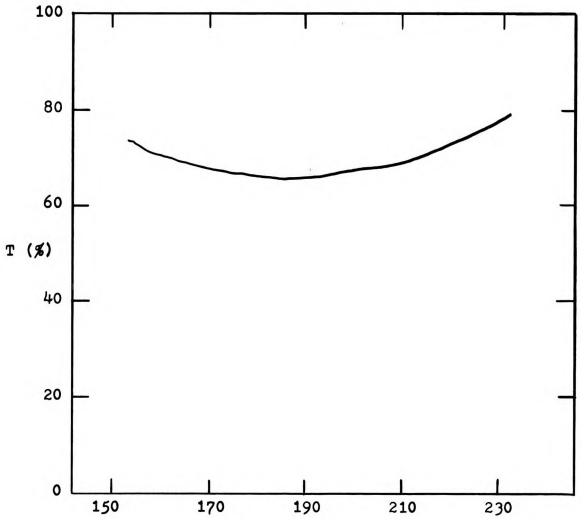

(Final)

40% LiBr-60% LiCl

Figure 20

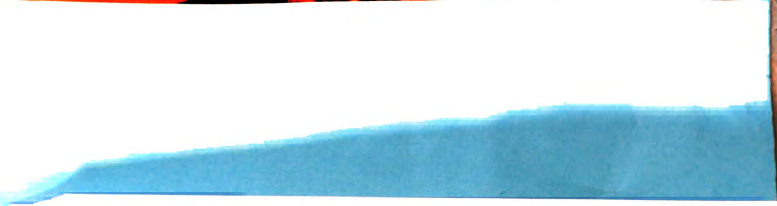

Fig

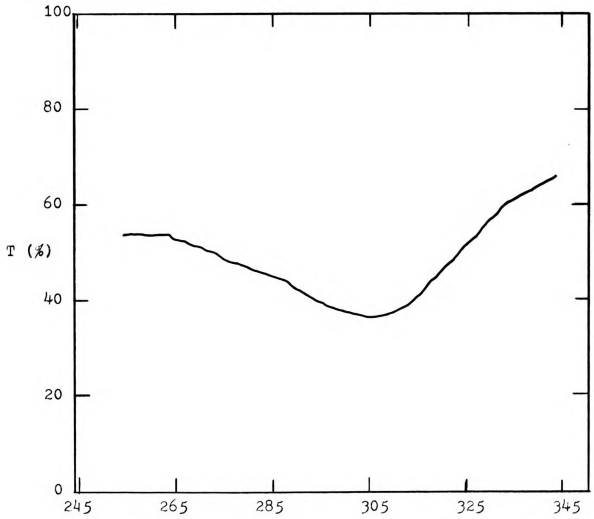
100
80
60
40
20
0
T (%)
245
265
285
305
325
345
Frequency (cm-1)
(Initial)
20% LiBr-80% LiCl

Figure 21

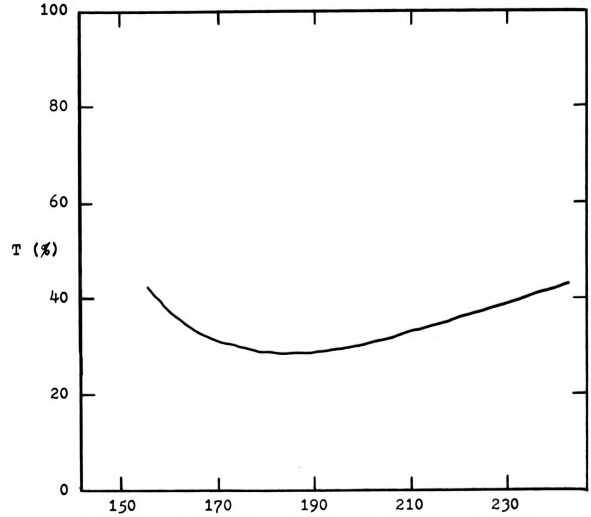
100
80
60
T (%)
40
20
0
150
170
190
210
230
Frequency (cm^{-1})
(Final)
20% LiBr-80% LiCl

Figure 22

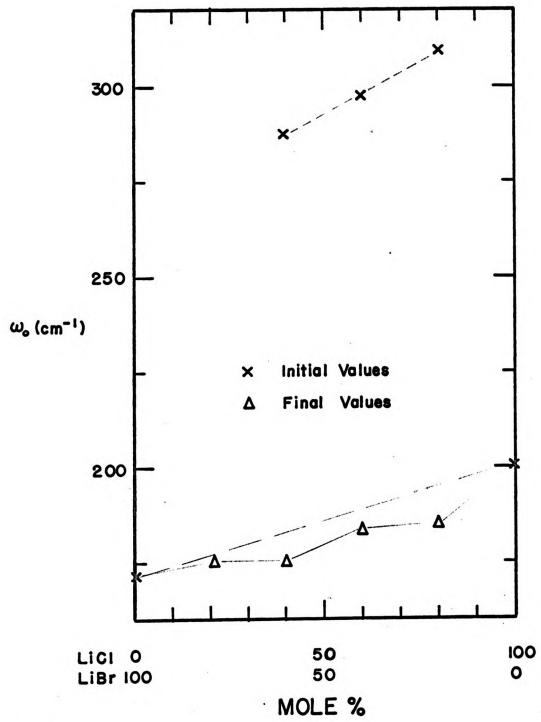
300
250
200
ω_o (cm^{-1})
× Initial Values
Δ Final Values
LiCl 0
LiBr 100
50
50
100
0
MOLE %

Figure 23

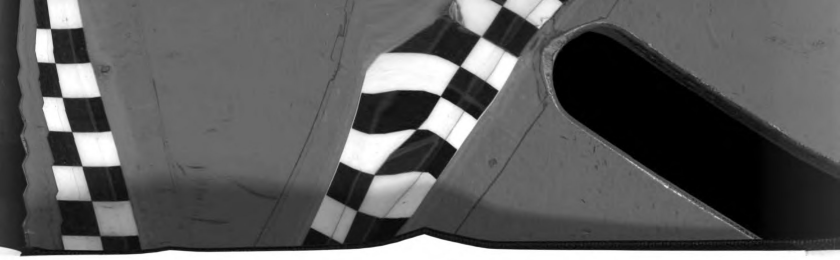

system was the only one studied at low temperatures, it is important to note the increased sharpness of the peaks and the upward shift of the dispersion frequency at low temperatures. The spectra obtained from the different compositions of this system show a broadening of the absorption peak as the melt mixture approaches 50%-50% both at room temperature and at liquid-nitrogen temperature. In this system there also appears to be a greater broadening with the 5% KI-95% NaI than with 5%NaI -95%KI mixture. (cf. figures 25 and 30)

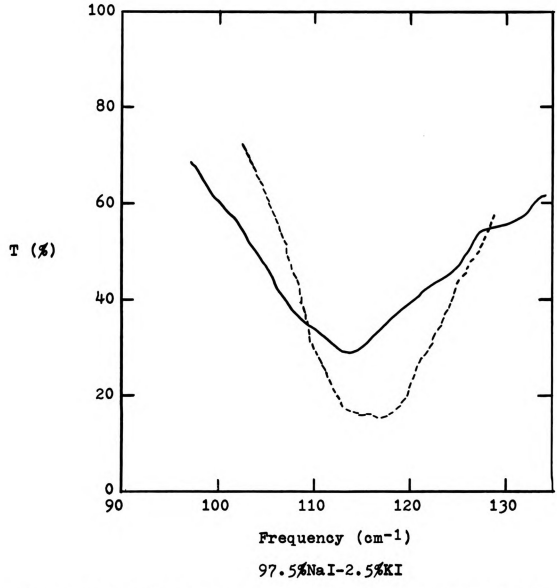

Figure 24 The solid line represents room temperature data, and the broken line the 110°K data.

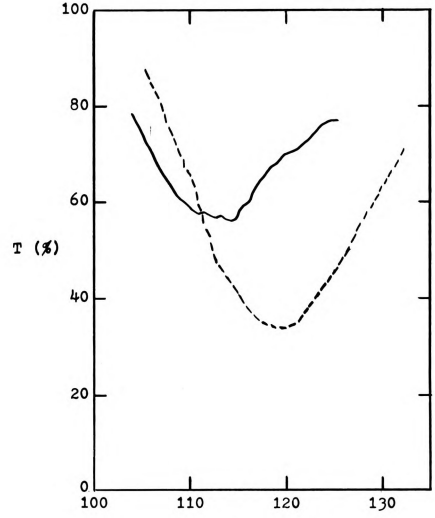

Figure 25 The solid line represents the room temperature data, and the broken line the 110°K data.

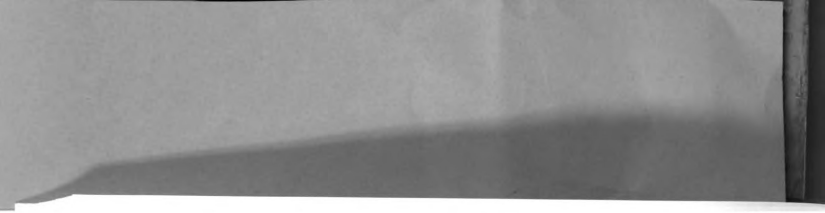

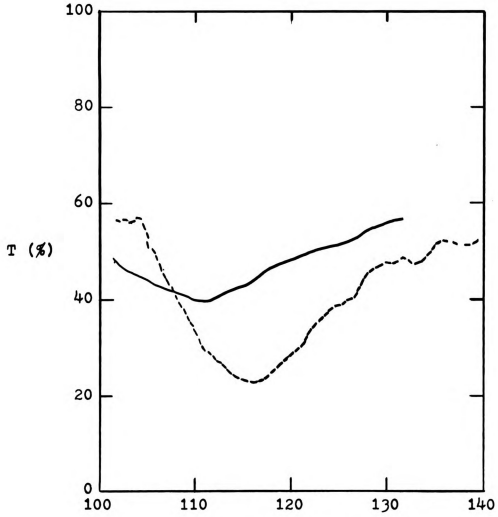

Figure 26 The solid line represents room temperature data, and the broken line the 110°K data.

Fig

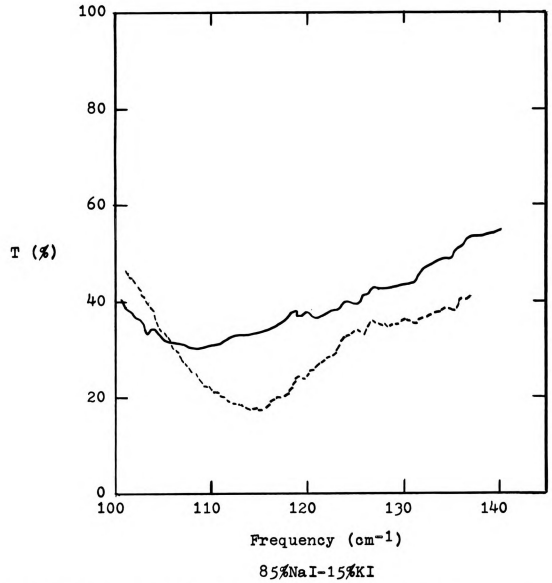

Figure 27 The solid line represents room temperature data, and the broken line the 110°K data.

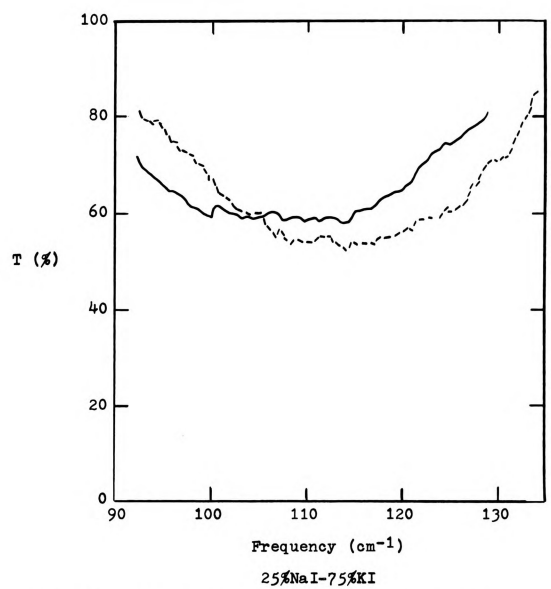

Figure 28 The solid line represents room temperature data, and the broken line the 110°K data.

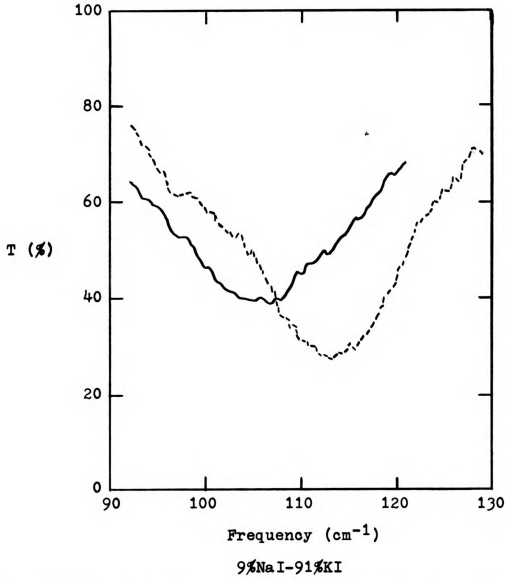

Figure 29 The solid line represents room temperature data, and the broken line the 110°K data.

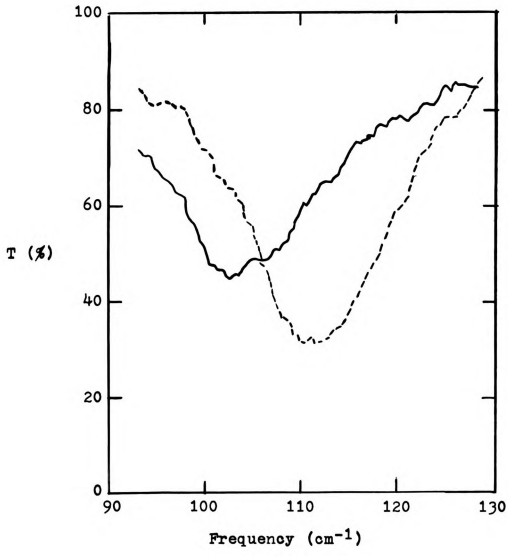

Figure 30 The solid line represents room temperature data, and the broken line the 110°K data.

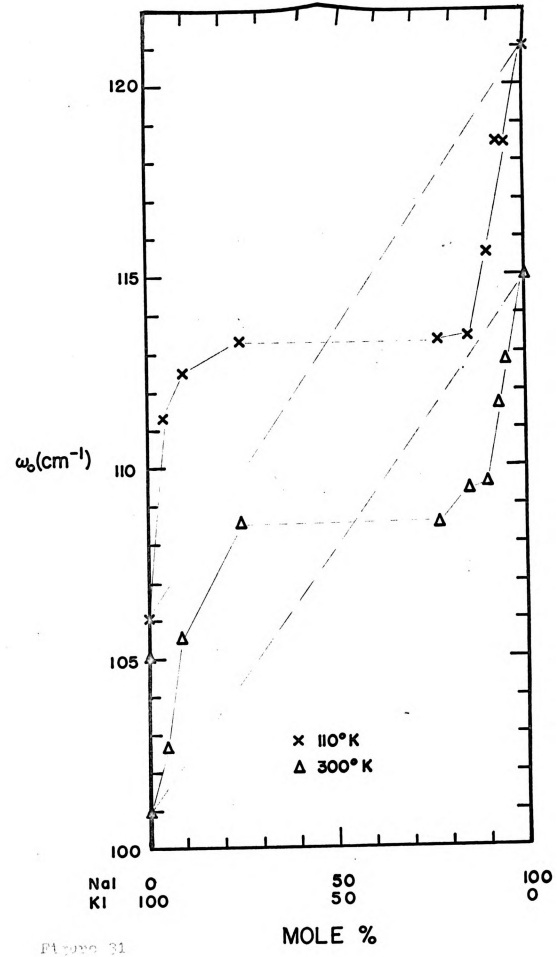
120
115
110
105
100
$\omega_o(cm^{-1})$
× 110°K
Δ 300°K
NaI 0 50 100
KI 100 50 0
MOLE %

Figure 31

General Discussion

Two aspects of the experimental results need discussion. First, the dispersion frequency and its dependence on composition and temperature of the films; and second, the shape of the spectra as it changes with composition and temperature of the film.

Infrared Dispersion Frequency

We have defined the dispersion frequency as the frequency at the minimum of the transmission spectra. The values of the dispersion frequencies are plotted for each of the systems studied in figure 15 (LiBr-NaBr), figure 23 (LiBr-LiCl), and figure 31 (NaI-KI) as a function of the composition of the melt in the boat during evaporation.

First it is in order to check on the pseudoisotopic character of these systems. The simple model of lattice vibrations shows that the infrared dispersion frequency is proportional to the inverse of the square root of the isotopic mass. Actually, comparisons should be made at the same reduced temperature T/Θ, where Θ is some characteristic temperature. The dispersion frequencies vary only slightly with temperature, however, and we will make comparisons at the same actual temperature. Comparison of the ratios of the dispersion frequencies ω/ω_0 with the appropriate reduced mass ratios $(\mu_0/\mu)^{1/2}$ are shown in tables III through VIII. It is clear that our naive

TABLE III Effect of composition on dispersion frequency for NaI-KI films with ω_o and μ_o from NaI as reference.

Composition	ω (cm^{-1})	ω/ω_o	$(\mu)^{1/2}$	$(\mu_o/\mu)^{1/2}$
NaI	115	1.00	4.42	1.00
95%NaI-5%KI	112	0.97	4.48	0.99
90%NaI-10%KI	110	0.96	4.54	0.97
80%NaI-20%KI	109	0.95	4.66	0.95
60%NaI-40%KI	108.5	0.94	4.89	0.90
20%NaI-80%KI	108	0.94	5.29	0.84
10%NaI-90%KI	105.5	0.92	5.38	0.82
5%NaI-95%KI	102.5	0.89	5.42	0.81
KI	101	0.88	5.48	0.80

TABLE IV Effect of composition on dispersion frequency for NaI-KI films with ω_o and μ_o from KI as reference.

Composition	ω (cm^{-1})	ω/ω_o	$(\mu)^{1/2}$	$(\mu_o/\mu)^{1/2}$
KI	101	1.00	5.48	1.00
5%NaI-95%KI	102.5	1.02	5.42	1.01
10%NaI-90%KI	105.5	1.04	5.38	1.02
20%NaI-80%KI	108	1.07	5.29	1.04
40%NaI-60%KI	108.5	1.07	5.10	1.08
80%NaI-20%KI	109	1.08	4.66	1.18
90%NaI-10%KI	110	1.09	4.54	1.21
95%NaI-5%KI	112	1.11	4.48	1.22
NaI	115	1.14	4.42	1.24

TABLE V Effect of composition on dispersion frequency for LiBr-NaBr films with ω_o and μ_o from LiBr as reference.

Composition	$\omega(cm^{-1})$	ω/ω_o	$(\mu)^{1/2}$	$(\mu_o/\mu)^{1/2}$
LiBr	171	1.00	2.53	1.00
90%LiBr-10%NaBr	158	0.92	2.80	0.90
83%LiBr-17%NaBr	157	0.92	2.94	0.86
75%LiBr-25%NaBr	152	0.89	3.10	0.82
30%LiBr-70%NaBr	139	0.81	3.85	0.66
21%LiBr-79%NaBr	139	0.81	3.98	0.64
10%LiBr-90%NaBr	137	0.80	4.11	0.62
NaBr	135	0.79	4.22	0.60

TABLE VI Effect of composition on dispersion frequency for LiBr-NaBr film with ω_o and μ_o from NaBr as reference.

Composition	$\omega(cm^{-1})$	ω/ω_o	$(\mu)^{1/2}$	$(\mu_o/\mu)^{1/2}$
NaBr	135	1.00	4.22	1.00
10%LiBr-90%NaBr	137	1.02	4.11	1.03
21%LiBr-79%NaBr	139	1.03	3.98	1.06
30%LiBr-70%NaBr	139	1.03	3.85	1.10
75%LiBr-25%NaBr	152	1.13	3.10	1.34
83%LiBr-17%NaBr	157	1.16	2.94	1.43
90%LiBr-10%NaBr	158	1.17	2.80	1.50
LiBr	171	1.27	2.53	1.67

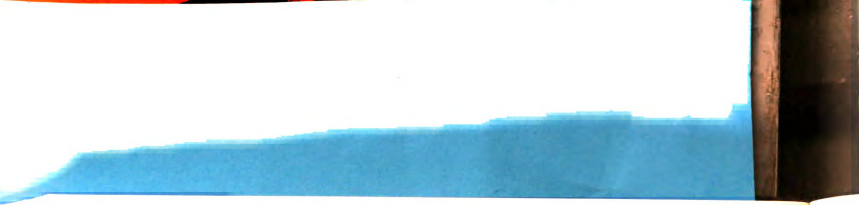

TABLE VII Effect of composition on the dispersion frequency for LiCl-LiBr films with ω_o and μ_o from LiBr as reference.

Composition	ω	ω/ω_o	$(\mu)^{1/2}$	$(\mu_o/\mu)^{1/2}$
LiBr	171	1.00	2.53	1.00
79%LiBr-21%LiCl	174	1.02	2.51	1.01
60%LiBr-40%LiCl	176	1.03	2.50	1.01
40%LiBr-60%LiCl	181	1.06	2.48	1.02
20%LiBr-80%LiCl	189	1.11	2.45	1.03
LiCl	201	1.18	2.41	1.05

TABLE VIII Effect of composition on the dispersion frequency for LiCl-LiBr films with ω_o and μ_o from LiCl as reference.

Composition	ω	ω/ω_o	$(\mu)^{1/2}$	$(\mu_o/\mu)^{1/2}$
LiCl	201	1.00	2.41	1.00
20%LiBr-80%LiCl	189	0.94	2.45	0.98
40%LiBr-60%LiCl	181	0.90	2.48	0.97
60%LiBr-40%LiCl	176	0.88	2.50	0.96
21%LiBr-79%LiCl	174	0.87	2.51	0.96
LiBr	171	0.85	2.53	0.95

pseudoisotopic assumption is not supported by these data for pure films. We still might expect, however, that for small amounts of impurity atoms replacing host alkali-halide atoms, we would find the reduced mass to be the dominant factor in determining the dispersion frequency for the mixed systems. In the tables we find reasonable agreement for films from melts containing small percentages of impurity atoms replacing host atoms. Films from mixtures containing a few percent of the heavier impurity atoms tend to have larger deviations from this pseudoisotopic characteristic for all of the systems studied. Although this shift of dispersion frequency is qualitatively in support of Hardy's (5) suggestion, no large shift of the dispersion frequency occurs for these small concentrations of impurities, as was observed for the LiH-LiD system (3). We note also that the frequency ratio is higher than the appropriate reduced-mass ratio for the LiBr-NaBr system and the LiBr-LiCl system when the minority component is the heavier constituent. In our simple model this relation implies a greater force constant or restoring force for the mixed films. For the NaI-KI system the frequency ratio is higher than the appropriate reduced-mass ratio when the minority component is the lighter NaI.

From the data of figure 31 we can determine the ratio of the dispersion frequency at 110°K to the dispersion frequency at room temperature for each of the combinations of the NaI-KI system that were studied. This ratio is

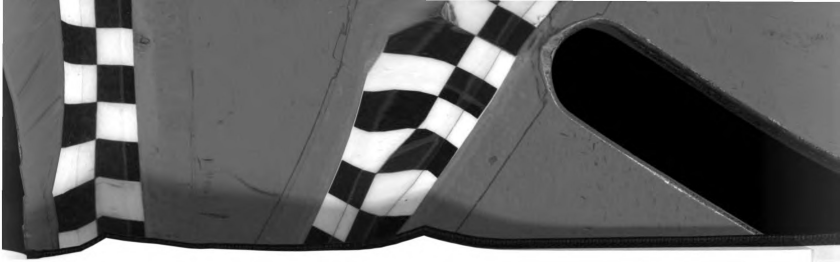

calculated to be 1.05 for each of the combinations. The constancy of this ratio is consistent with the pseudo-isotopic assumption made for small percentages of one alkali halide in a host film. For in this model, the reduced mass, which is independent of temperature, is the dominant factor in determining the dispersion frequency of the mixed film.

Absorption Spectra Shape

Although there is no complete theory for the structure of the absorption bands, we may gain some insight from observed differences in the shapes of the mixed film spectra as determined by composition and temperature. As pointed out before, a 97%LiBr-3%NaBr mixture, and similarly a 95%NaI-5%KI mixture, produce a much broader absorption band than does the 5%NaI-95%KI mixture. In both the LiBr-NaBr system and the NaI-KI system, a small percentage of the heavier component put into the lighter host produces a broader absorption band than the reverse combination. This observation may be interpreted in the following way. This broadening of the absorption band is accompanied by a non-isotopic shift in the dispersion frequency. This shift in turn may be interpreted as evidence of an anharmonic perturbation on our harmonic binding force. One of the many suggestions made to account for absorption band widths is that such anharmonicity would indeed give rise to secondary structure in the infrared absorption spectra.

In summary, this study has demonstrated the feasibility of getting meaningful data for all the alkali halides in pure form, and has pointed out promising areas for mixtures of alkali halides. There appears to be a correlation between the larger values of the damping parameter and the larger deviations of the e*/e Szigeti ratio from unity. This correlation deserves further study, both experimentally and theoretically. The information contained in the shape of the absorption spectra remains untapped. In the mixed-film spectra of this study there was some systematic variation of spectra shape as a function of both composition and temperature. As yet, however, we have no good theoretical interpretation of these observations. Further investigations of mixed films and pure films at low and high temperatures would provide further insight into the temperature dependence of the dispersion frequency and absorption spectra shape.

Data from other mixtures of alkali-halides containing no common constituents would provide additional information concerning the pseudoisotopic character of alkali-halide systems. For a thorough check of Hardy's (5) theoretical treatment of isotopic defects, an experimental study of the NaH-NaD system is needed.

References

1. R. B. Barnes, and M. Czerny, Z. Physik 72, 447 (1931); R. B. Barnes, Z. Physik 75, 723 (1932).
2. W. B. Zimmerman, Ph.D. Thesis, Mich. State. U. (1960)
3. R. H. Misho, Ph. D. Thesis, Mich. State U. (1961)
4. C. M. Randall, Ph.D. Thesis, Mich. State U. (1964)
5. J. R. Hardy, Phys. Rev. A136, 1745 (1964).
6. B. Szigeti, Proc. Roy. Soc. A204, 51 (1950).
7. H. M. Randall, D. M. Dennison, N. Ginsburg, and L. R. Weber, Phys. Rev. 52, 160 (1937).
8. K. N. Rao, R. V. deVore, and E. K. Plyler, J. Res. N. B. S. 67A, 351 (1963).
9. M. Hass, J. Phys. Chem. Solids 24, 1159, (1963).
10. G. O. Jones, D. H. Martin, P. A. Mawer, and C. H. Perry, Proc. Roy. Soc. A261, 10 (1961).
11. H. W. Hohls, Ann. d. Physik 29, 433 (1937)
12. R. G. Dick, Jr. and A. W. Overhauser, Phys. Rev. 112, 90 (1958).
13. E. E. Havinga, Phys. Rev. 119, 1193 (1960).
14. M. Born and K. Huang, 1954, Dynamical Theory of Crystal Lattices, Oxford, Clarendon Press.

APPENDIX

Adjusted Transmission Spectra for Pure Alkali-Halide Films

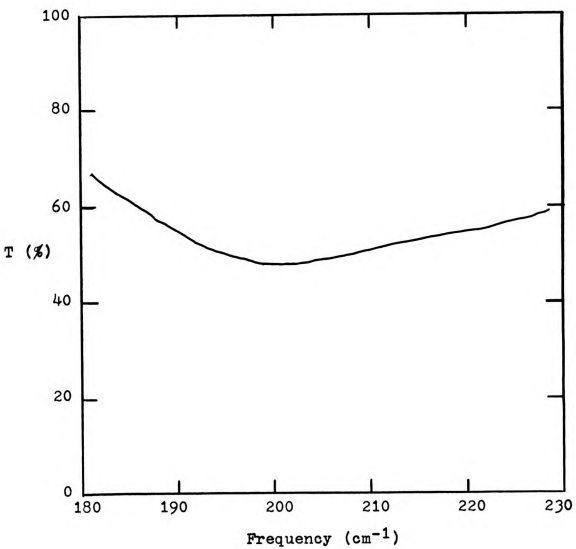

Figure 32

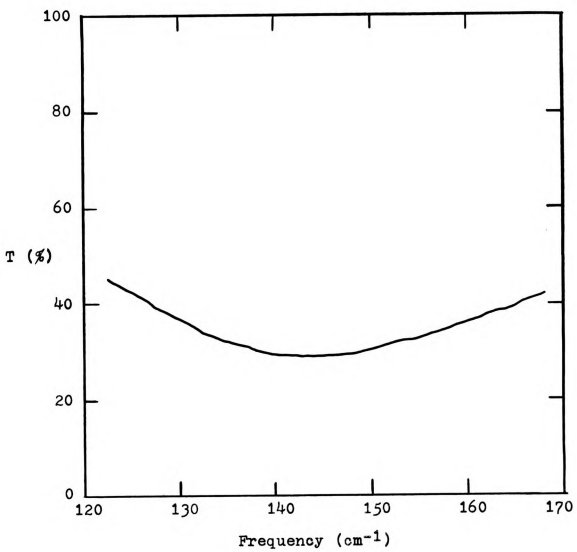

Figure 33

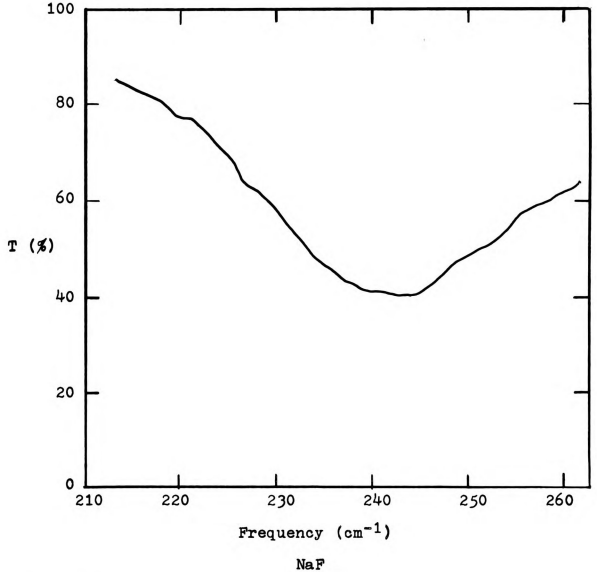

Figure 34

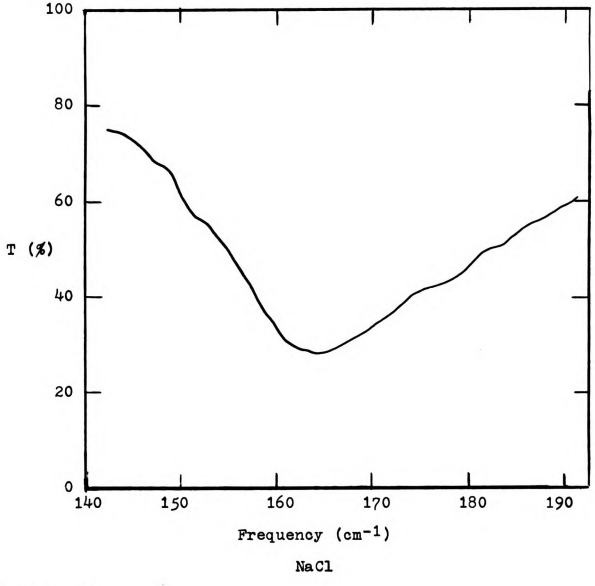

Figure 35

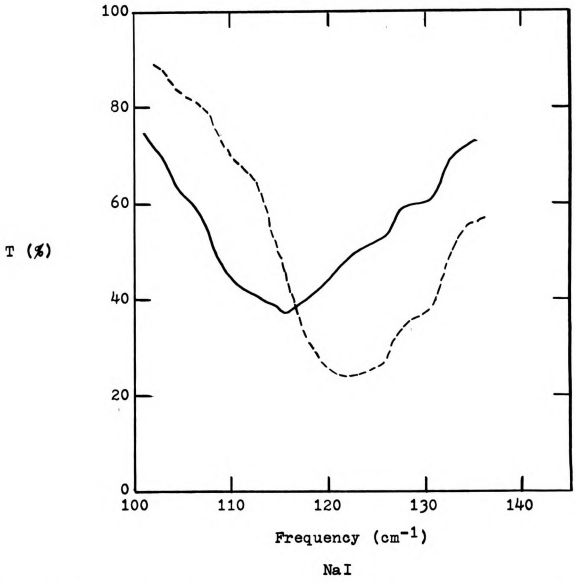

Figure 36 The solid line is room temperature data and the broken line is 110°K data.

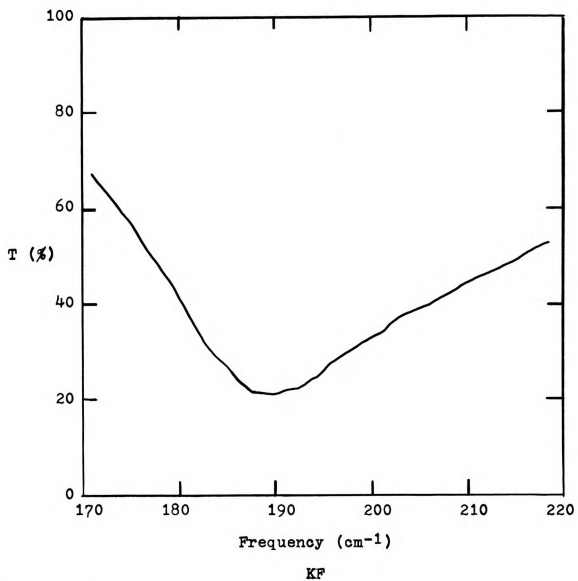

Figure 37

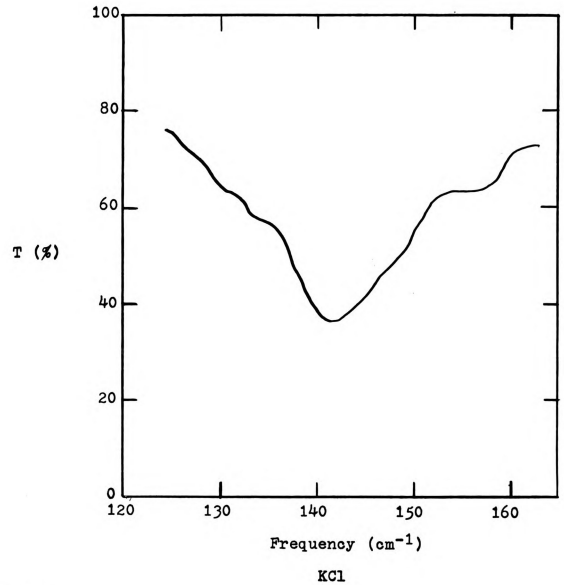

Figure 38

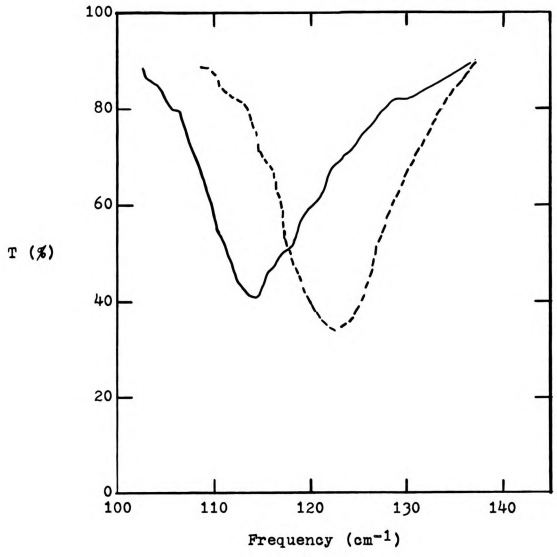

Figure 39 The solid line is room temperature data and the broken line is 110°K data.

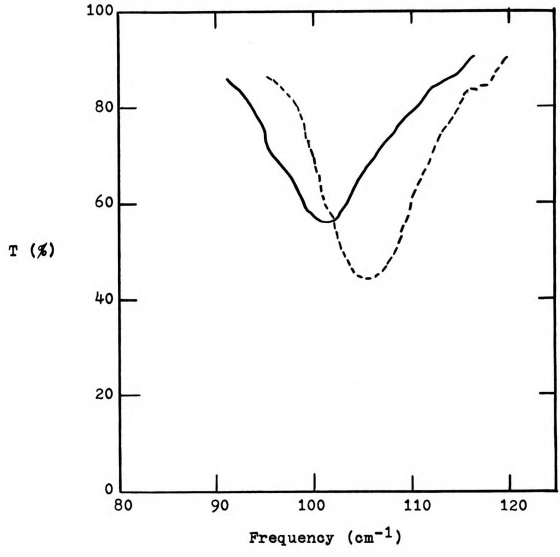

Figure 40 The solid line is room temperature data and the broken line is 110°K data.

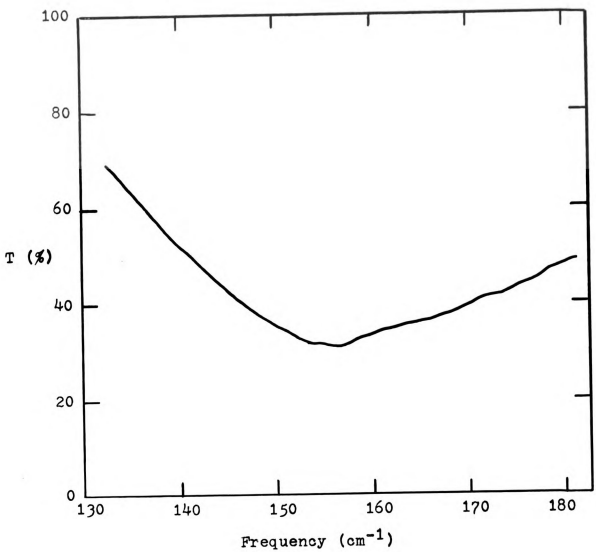

Figure 41

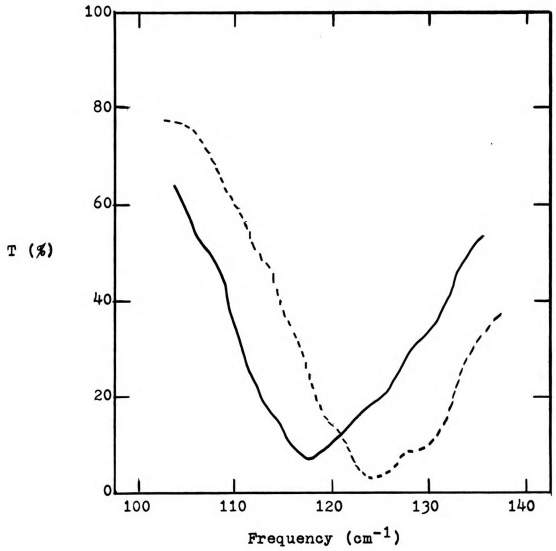

Figure 42 The solid line is room temperature data and the broken line is 110°K data.

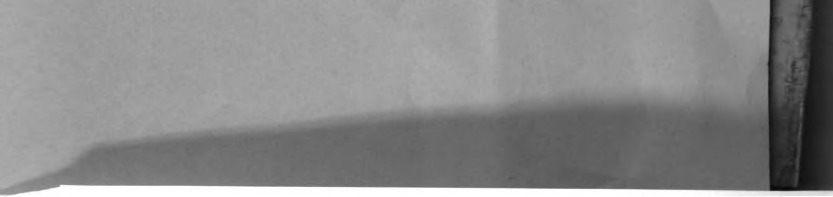

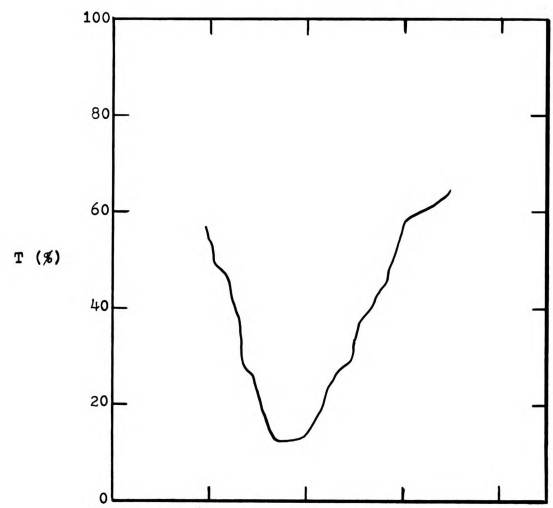

Figure 43

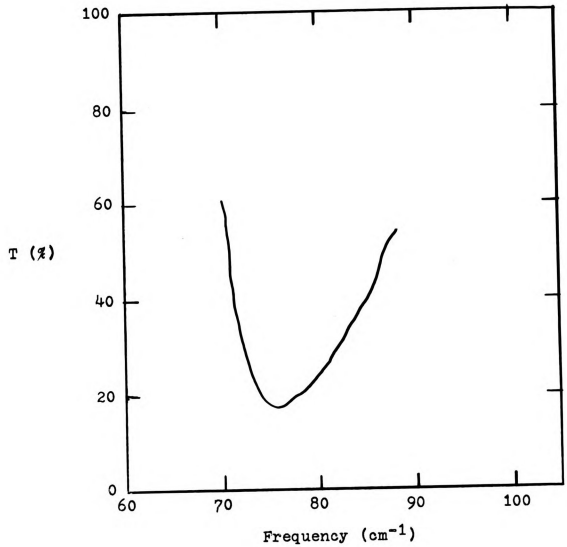

Figure 44

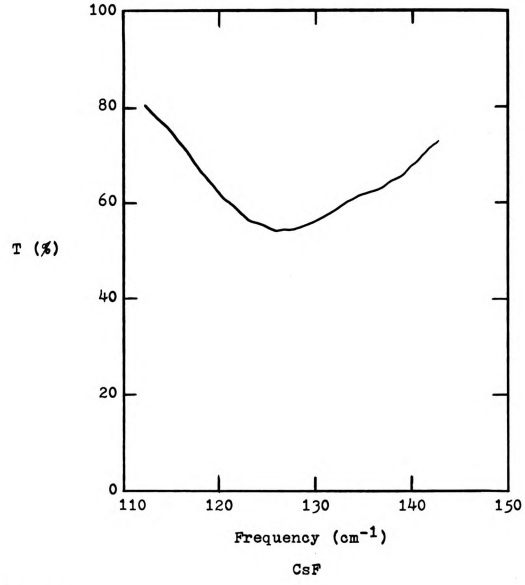

Figure 45

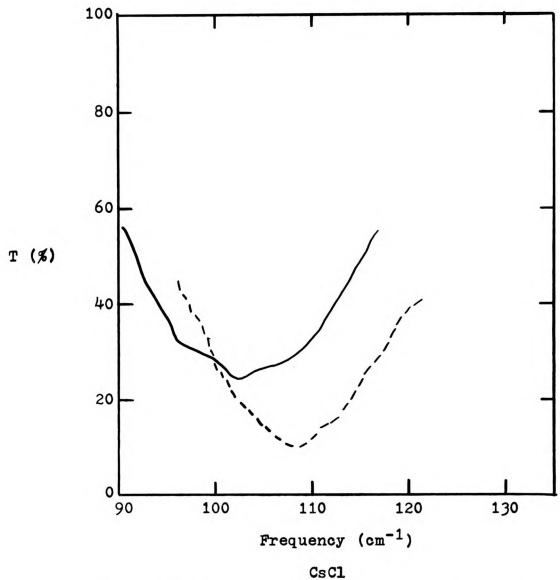

Figure 46 The solid line is room temperature data and the broken line is 110°K data.

T (K)
Frequency (cm^{-1})

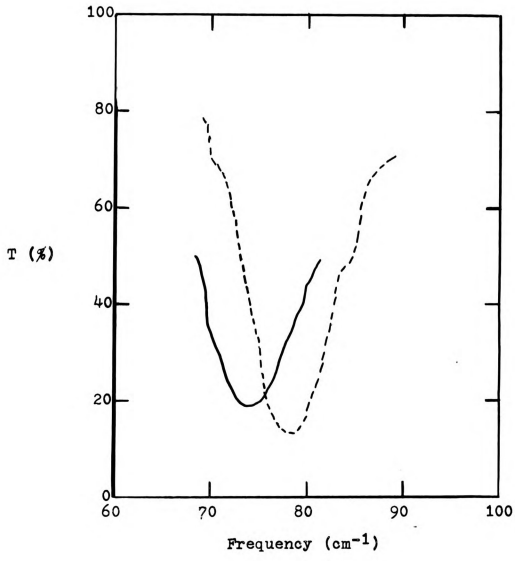

Figure 47 The solid line is room temperature data and the broken line is 110°K data.